universität wien

MASTERARBEIT / MASTER'S THESIS

Titel der Masterarbeit / Title of the Master's Thesis

„The XUV Sun in Time"

verfasst von / submitted by

Nina-Elisabeth Nemec, BSc

angestrebter akademischer Grad / in partial fulfilment of the requirements for the degree of

Master of Science (MSc)

Wien, 2017/ Vienna 2017

Studienkennzahl lt. Studienblatt / degree programme code as it appears on the student record sheet:	A 066 881
Studienrichtung lt. Studienblatt / degree programme as it appears on the student record sheet:	Masterstudium Astronomie
Betreut von / Supervisor:	Univ.-Prof. Dipl.-Phys. Dr. Manuel Güdel

Abstract

The evolution of the X-ray and extreme ultraviolet radiation (XUV) is important to understand the evolution of planetary atmospheres. The XUV output of solar-like stars varies with time, with a decay seen in all wavelength regimes. We put forward a new way of modeling the flux between 36-92 nm. Due to interstellar extinction is it not possible to measure fluxes in this regime for stars other than our Sun. We use solar spectral features that are co-added according to filling factors that are derived from the S-index, the latter traces the plage coverage. We find that our models are consistent with the literature and are able to study the effect of the variation in the S-index on the XUV spectra for our sample stars.

Acknowledgements

First and foremost I want to thank my supervisors Manuel, Theresa and Colin. You have helped shaping me into the scientist and student I am today. Even though your schedules have been full most of the time, you always took the time to meet and discuss science left and right. It was a pleasure to work with you and I hope that we will be able to work together as well in the future.

Another person whom has to be thanked is Juan Fontenla, for providing us the solar spectral features used in this work.

"Thank you" as well to all my colleagues and friends. We have gone trough a lot of trouble together. I am glad that some of you really became close friends and I hope that even though our ways are going to part now, we will always share a good connection.

Last, but not least, it was my parents, Michaela and Franz, and my sister Sarah, that made everything possible. You always took me the way I am and provided me with the environment that made it possible to focus on my studies. Especially my mother has helped me through a lot of harsh times in the past. Even though I sometimes was not the daughter you deserved you always supported me. When I was reaching for the stars, it was you, my family, that always backed me.

Contents

List of Figures

List of Tables

for my family

Chapter 1

Introduction

1.1 Motivation: Planet hosting stars

With the ground-breaking discovery of planets orbiting a star other than the Sun, namely, HD114762 (Latham et al., 1989) in 1989 and the confirmation of the first one in 1991 (Cochran, Hatzes, and Hancock, 1991) it was clear, that the Sun is not the only planet hosting star. In 1995 the first planet was discovered around the main sequence star 51 Peg (Mayor and Queloz, 1995). This star was found to have a companion, that is 11 times heavier than Jupiter, but this planet orbits around its host star at a distance smaller than Mercury's orbit. These so-called "hot Jupiters" have challenged the view on how planet systems are formed and how different planets are distributed in comparison to our own planet system. New and better detection methods soon allowed to hunt for exoplanets in the habitable zone, that is, the zone around a host star, where liquid water can potentially exist on the surface of a planet. The first Earth-mass exoplanet in the habitable zone of its host star was announced in 2014 by NASA. Since then, many more planets with the size of the Earth have been discovered and confirmed. Just the *Kepler* mission alone as of April 28,2017 has found 4496 exoplanet candidates, 2335 confirmed exoplanets out of which 21 are less then twice the size of Earth in a habitable zone.

The *K2* mission, initiated in 2014, when 2 of the 4 reaction wheels of the satellite failed, has found 520 candidate and 147 confirmed exoplanets as of April 28,2017.
The definition of a habitable zone and the range of where liquid water could exist is not a new idea, but of course the following question has the be asked: *What makes a planet habitable?* On Earth we know, that water was a main ingredient, but also an atmosphere, a magnetic field, a stable orbit, a moon, land masses, stable weather conditions, etc. may be important to bring up life.

However, not only the properties of the planet are important, but also its host star must fulfill certain conditions. From the Sun and our own planet, we know that a long, stable hydrogen burning phase is needed, in order to give life enough time to develop. Also the activity of the star plays a role. Stellar winds and the high energy radiation (X-ray to UV) have an impact on the planet, as they influence the atmosphere strongly. Strong stellar winds and a high dose of high energy radiation can speed up atmospheric escape mechanisms, even reaching a point where a planet is stripped off high initial hydrogen envelope. Then the question arises, if the planet is able to out-gas a secondary atmosphere. One can of course add endless factors to the list of what makes a planet habitable further.

1.2 Importance of rotational evolution of the host star

The X-ray and extreme-ultraviolet (XUV) radiation is an important factor regarding both the evolution of the star and the planet's atmosphere itself. Planets form with an initial hydrogen envelope and it depends on the stellar XUV radiation, how both the primordial hydrogen atmosphere (eg. Lammer et al., 2014), and also the secondary nitrogen atmosphere (Lichtenegger et al. (2010)) evolves with time. XUV radiation drives the chemistry of atmospheres (Tian et al., 2008; Koskinen et al., 2013, Shaikhislamov et al., 2014; Shematovich, Ionov, and Lammer, 2014;Chadney et al., 2015) and causes heating that leads to an expansion of the atmosphere and consequent mass loss (Tian et al., 2005; Erkaev et al., 2013, Luger et al., 2015). In addition to the high energy radiation, stellar winds drive additional non-thermal loss processes (e.g. ion pick-up, Kislyakova et al., 2013; Kislyakova et al., 2014).

The evolution of the XUV radiation is primarly coupled to the rotation period, except when the star is in the so-called saturation regime Wright et al. (2011). However, stars in young stellar clusters show a wide range of rotation rates, before they converge to a unique mass-dependent value Soderblom et al. (1993). This means that stellar activity evolution is not solely determined by the stellar mass and age, but on its initial rotational period (Johnstone et al., 2015;Tu et al., 2015). As a consequence of the initial rotation period,the duration of the saturation regime may range between 10 and several hundred Myr. With the X-ray luminosity being coupled to the activity and thus age, young stellar clusters also show a wide distribution in L_X. Tu et al., 2015 and Johnstone et al., 2015 developed a rotational evolution model to predict such luminosity distributions. Fig. 1.1 shows different evolutionary tracks and the dependence of L_X and L_{EUV} and the rotational period. Therefore, caution should be taken when considering atmospheric evolution, as the stellar XUV evolution itself depends on initial rotation period and the related evolutionary track.

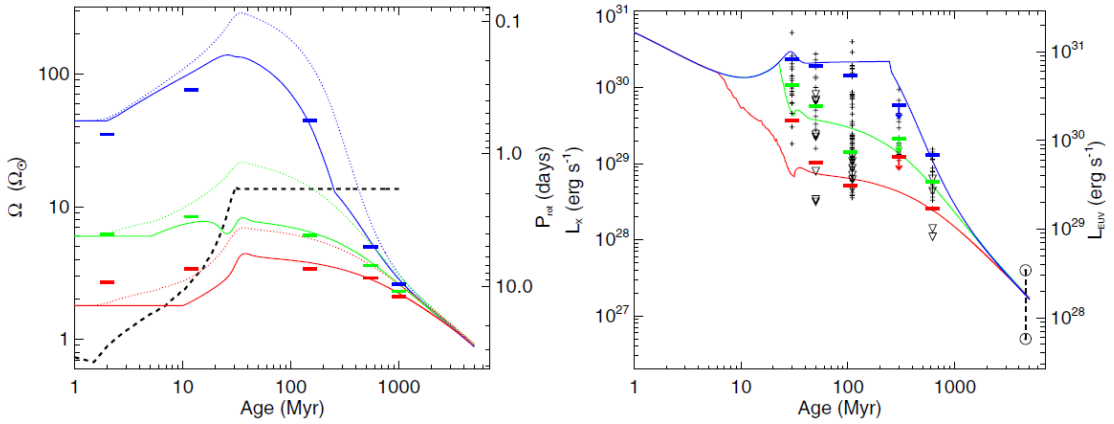

FIGURE 1.1: Left: Models for rotational evolution tracks for stars of different percentiles (red: 10th, green: 50th, blue: 90th). Dashed lines show the core rotational evolution, solid lines the rotational evolution of the envelope. Right: Predicted L_x of the evolutionary tracks in comparison with measurements from cluster stars. (Taken from Tu et al., 2015)

Johnstone et al. (2015) highlited again the importance of the rotational evolution of the host star. Fig. 1.2 shows results from this study. A hydrodynamic model was used for the upper atmosphere, a hydrostatic model for the lower atmosphere and only hydrogen was considered. It is clearly illustrated that the number density of the escaping

particles depends on the integrated XUV-flux. The number density is dependent on the temperature (Fig. 1.2 right), where the higher fluxes heat the atmosphere to higher temperatures. Also noticeable is that the mass that is escaping is not linearly coupled to F_{XUV}.

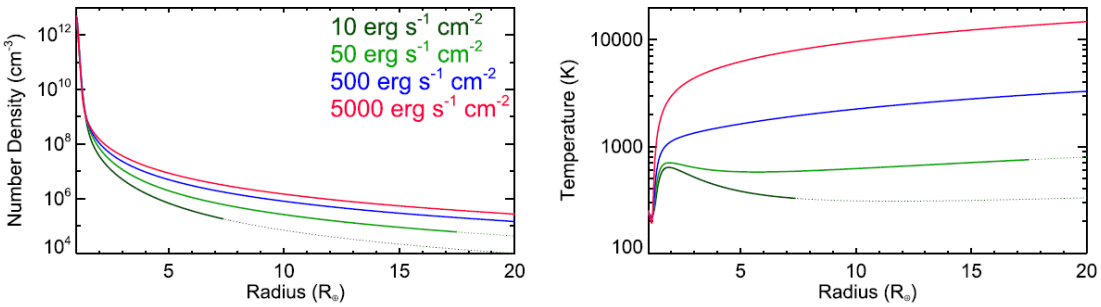

FIGURE 1.2: Hydrodynamic models of the expansion of the upper atmosphere for a Earth mass planet. Left: Hydrogen density, right: temperature profile. See text for more details (Taken from Johnstone et al 2015)

F_{XUV} is important for the total mass loss, but Guo and Ben-Jaffel (2016) have shown that the stellar EUV spectral energy distribution (SED) plays a more important role on the physical and chemical properties of the escaping atmospheres. On the other hand the stellar EUV SED only affects the total mass loss little. Different profiles of EUV SEDs can dramatically change the composition and species distribution of the escaping atmosphere. Photoionization at different altitudes have shown to vary between 1-2 orders of magnitudes depending on the shape of the stellar EUV SED. If the EUV SED is dominated by the 40-90 nm regime, photoionization of H is prominent on lower altitudes in the atmosphere, whereas if the 0.5-40 nm regime dominates the transition from H to H^+ moves to higher altitudes. Moreover, that atmospheric evolution is also in dependence of the hydrodynamic escape parameter (λ). At low λ, the resulting low temperature of the atmosphere makes other chemical reactions important so that photoionization can no longer determine the composition of the escaping atmosphere.

Having named different channels through which the interaction between the host star and its planet can happen and their influence on the planet itself, we again want to stress that no atmospheric escape model will work properly if 1) the X-ray and extreme ultraviolet (XUV) flux of the host star is not properly characterized, 2) the stellar rotational evolution is not known and 3) the atmospheric composition of the planets atmosphere is unknown.

1.3 Solar-like stars, solar analogs and solar twins

In the present work we want to study the X-ray and extreme-ultraviolet evolution of solar like stars. We therefore take the "classical" young solar analogs EK Dra, π^1 UMa and β Com and use a new method to model their spectra. But what exactly makes are star a solar type star, a solar analog or even a solar twin? We will follow the definitions given in Cayrel de Strobel (1996).

Generally, solar-like or solar-type stars are collective terms for stars, that are similar in mass and are at a similar evolutionary stage. It is defined for stars with a convective envelope, that arises below 2.3 $M_\odot$, but since those stars have a radiative core, so

that definition excludes M dwarfs that are mostly dominated by convective zones. Solar analogs are stars with detailed properties that are similar to the Sun's. This includes the same (photometric) temperature within a broader limit and a metallicity within a factor of 2 difference. Moreover, those stars have to be in the hydrogen burning phase, which excludes evolved stars and stars that are not yet on the main sequence. Also close binaries are not considered in this term, as tidal effects affect the evolution of those stars (Mathieu and Mazeh, 1988). Close binaries can spin up again, which means that at a certain point the rotation period is decoupled from age and also the activity of those stars in enhanced. The term solar twin describes stars that have a temperature close to the Sun (10 K difference), the same metallicity within 0.05 dex, an age within 1 Gyr and no known stellar companion, as the Sun is considered to be a single star as well. In the present work we consider a young solar analog any star that has a similar radius, similar mass and similar spectral type (at least G-type), but we ignore the aspect of our sample stars requiring the age of the Sun. This is because we want to study, how the X-ray and extreme-ultraviolet radiation changes over stellar evolution. Our sample consists of 3 young solar analogs with ages of 0.1, 0.3 and 1.6 Gyr and the Sun.

We will start discussing the coronal and chromospheric evolution of cool stars in Sec.1 and follow in Sec.2 a summary on how to model the solar spectrum focusing solely on the visual wavelength regime. In this section we also want to discuss photometric variability of solar type stars and consider various ways of probing spots on stars other than the Sun. As the stage is set, we will present in Sec.3 the works by Juan Fontenla and his collaborators that lead to the development of the spectra used in this work. Sec.3 also contains the obtained scaling relations, which will give us the filling and weighting factors for the mentioned components. Finally, Chapter 5 presents and hold the results, that are broadly discussed in Sec.5, where we study in detail the effect of plage and spot coverage.

Chapter 2

The coronae and chromospheres of cool stars

2.1 The corona

2.2 Coronal evolution

The corona is the part of the stellar atmosphere with the lowest density, but the highest temperature. With 1-20 MK it is significantly hotter than the photosphere, however, it is still not well understood what heats the corona to these temperatures. Due to the the high temperature one the corona is composed of highly ionized particles, and magnetic fields also play an important role in the corona. As it is hard to study magnetic field in stars other than the Sun, the coronal X-ray emission can give us hints on their magnetic fields of those. Understanding the magnetic field can help us understand other evolutionary effects of stellar evolution. The magnetic fields drive mass loss and during their evolution stars will eventually spin down due to magnetic braking and angular momentum transfer. The magnetic field also evolves, meaning that older low-mass stars have a weaker internal dynamo and show reduced magnetic activity (Skumanich, 1972).

It is believed that the Sun as it reached the zero main age sequence (ZAMS) was 25 % fainter than nowadays, but it was over 100 times more active in X-ray and the ultraviolet regime. The ZAMS is defined as the region in the Hertzsprung-Russell diagram, where stars firstly ignite the core hydrogen burning. Ribas et al. (2005) have shown that solar-like stars undergo decay over several wavelength regimes, though that decay changes from regime to regime. The most drastic changes are seen in the X-rays. EK Dra at 100 Myr of age has an X-ray output $\approx$ 1000 times the present Sun (Güdel, Guinan, and Skinner, 1997; Telleschi et al., 2005). However, it has to be noted that the solar luminosity varies between $\approx 10^{27}$ and $\approx 10^{26}$ erg/s from cycle maximum to cycle minimum (Peres et al., 2000).

The evolution with age in the X-rays is connected to several other lines in the longer wavelength regime. Ayres et al. (1995) reported relations between the X-rays from 0.1-2.4 keV and lines such as CIV and MgII. CIV and MgII are both lines that are dominated by chromospheric emission. The relation between the luminosity of those two lines and the X-ray luminosity is the following;

$$\frac{L_x}{L_{bol}} \approx \left(\frac{L_{CIV}}{L_{bol}}\right)^{1.5} \tag{2.1}$$

$$\frac{L_x}{L_{bol}} \approx \left(\frac{L_{MgII}}{L_{bol}}\right)^{3} \tag{2.2}$$

We mentioned that corona depends on the magnetic energy that is available, which makes the X-ray output depended on the dynamo. Stars slow down as they age and the age is coupled with the X-ray flux through (Maggio et al., 1987; Güdel, Guinan, and Skinner, 1997)

$$L_X \approx (3 \pm 1) \cdot 10^{28} t_9^{-1.5 \pm 0.3} \quad [\text{erg s}^{-1}] \tag{2.3}$$

where t_9 is the stellar age in Giga-years. Note that Eq. 2.3 only holds for solar like MS stars if they are not saturated ($L_x \leq 4 \cdot 10^{30}$ erg s^{-1}) and the rotation period and stellar age are coupled. Last condition occurs at $\approx$ 100 Myr (Soderblom et al., 1993).

$$L_X = 1031.05 \pm 0.12 P^{-2.64 \pm 0.12} \quad [\text{erg s}^{-1}] \tag{2.4}$$

We have mentioned that the coronal emission decays with age already, so we now want to look at this in more detail. Eq.2.4 gives a relation between rotation period and X-ray luminosity for solar like stars. Fig.2.1 shows the sample stars from Telleschi et al. (2005) . From top to bottom the stars become less active in X-rays, as L_X decreases with stellar age and increasing rotation period.

In Fig. 2.1 a shift in the fluxes from hard to soft X-ray can be seen. The youngest stars, 47 Cas B and EK Dra, show strong lines in the hard X-rays, which do not occur in for instance in β Com. indicates that for solar analogs at different ages, the coronal temperatures evolve. 47 Cas B and EK Dra show strong lines from highly ionized Fe and NeX. In order for these lines to be formed a plasma has to reach temperatures of order 10 MK. The least active star in this sample, β Com on the other hand, exhibits strong lines of Fe XVII, Ne IX, and O VII that dominate. For those lines only 2-5 MK are needed for formation. So not only L_X but also the coronal temperature evolves over time. Johnstone and Güdel (2015) investigated the average coronal temperatures of low-mass stars and found that the coronal flux F_X is the best indicator of coronal temperature. Fig.2.2 shows F_X against the coronal temperature for low mass main-sequence stars. 47 Cas B, EK Dra, as well as π^1 UMa and κ^1 Cet can be found at high F_X, whereas the Sun at cycle minimum and β Com are located at the low F_X regime.

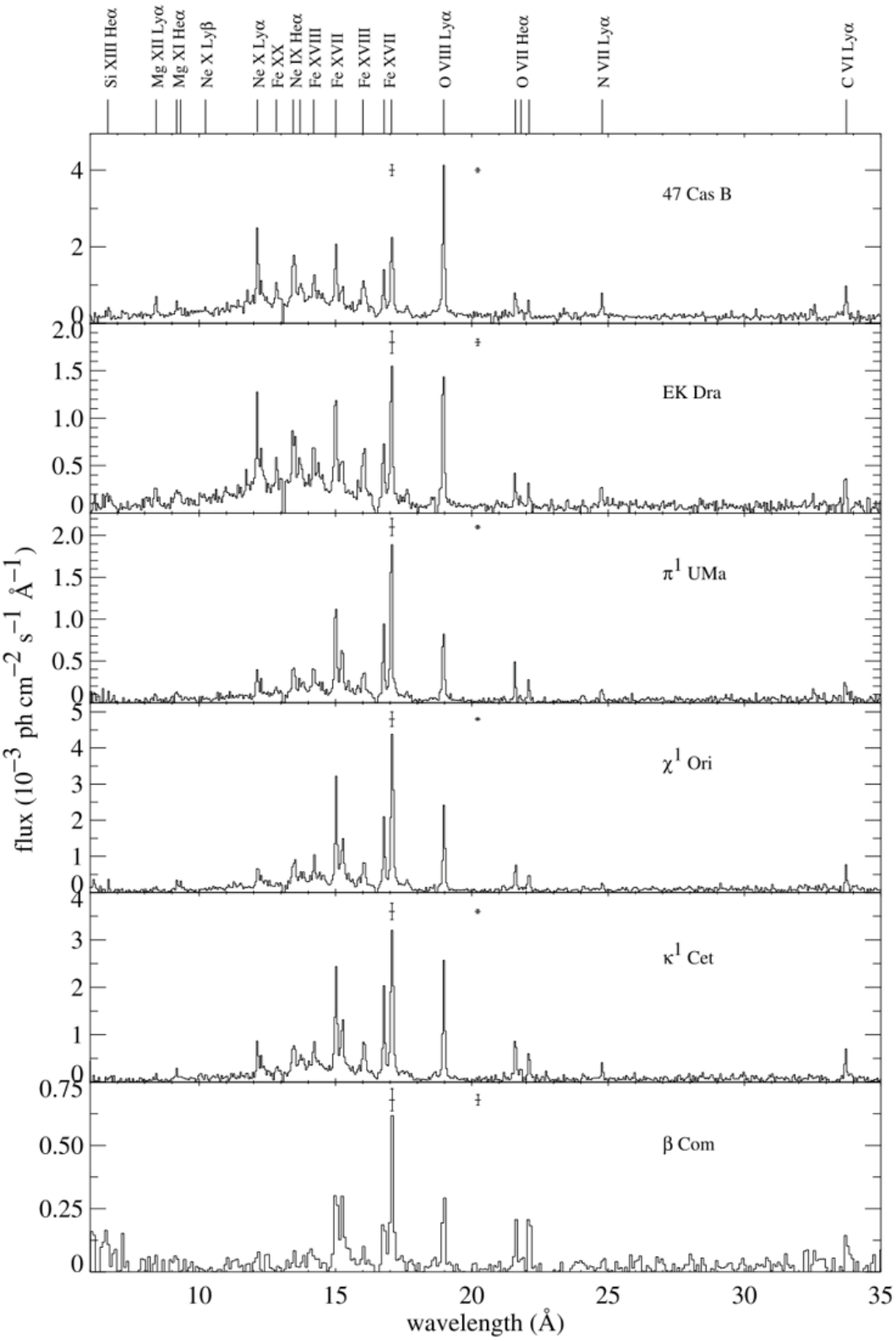

FIGURE 2.1: Spectra of a sample of young solar analogs. (From Telleschi et al., 2005.)

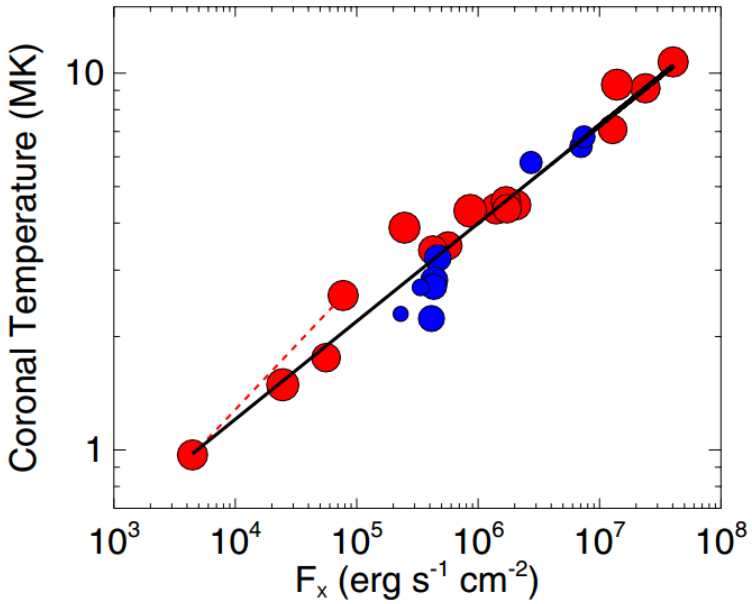

FIGURE 2.2: Average coronal temperature against X-ray flux (F_X). Blue and red represent stars with masses below and above 0.65 M_{odot} respectively. The dotted line connects the Sun from minimum to maximum. (From Johnstone and Güdel, 2015

2.2.1 Coronal modeling

Emission Measure Distributions (EMD) are another way of characterizing the emissivity of plasmas, hence stellar coronae. The observed flux of a line from an atomic transition line can be written as

$$\Phi_j = \frac{1}{4\pi d^2} \int A G_j(T) \frac{n_e n_H dV}{dlnT} dlnT \tag{2.5}$$

where Φ_j is the observed flux in a given line, d the distance, A the elemental abundance, $G_j(T)$ the line cooling function, n_e the electron and n_H the hydrogen number density. For fully ionized plasmas $n_H = 0.85 n_e$. The emission measure (EM) itself is proportional to the integral of N_e^2, hence the flux in Eq. 2.5 is given as the EM of a plasma multiplied by a cooling function. If an X-ray spectrum was to be modeled with an optically thin plasma, the EM is a free parameter.

Another quantity often used is the differential emission measure (DEM) that is given by

$$Q(T) = \frac{n_e n_H dV}{dlnT} \tag{2.6}$$

Eq. 2.6 is already included in 2.5 and both basically give a relation between the stellar X-ray observations (Φ_j) and the model of a thermal source (DEM, T). The equations take into account elemental abundances, densities and temperature of a emitting source. EM is a free parameter used for normalization, but but it give some constraints on for instance heating mechanisms and the temperature of sources. As can be seen in Fig. 2.3 for the emissivity of Fe and O, lines can form over a broad range in temperature. This makes the equations mentioned above to a certain degree degenerate. Different ionization states of both elements can be achieved at different temperatures, which usually span over a factor of two. Fig. 2.4 shows EMs of solar analogs. It is noticeable, that with higher ages (47 Cas B is the youngest star in this sample, β Com the oldest), both the

emissivities and the temperatures decrease, which is another hint on the evolution of stellar X-ray fluxes and coronae in time. For further reading on the X-ray astronomy of stellar coronae see Güdel (2004).

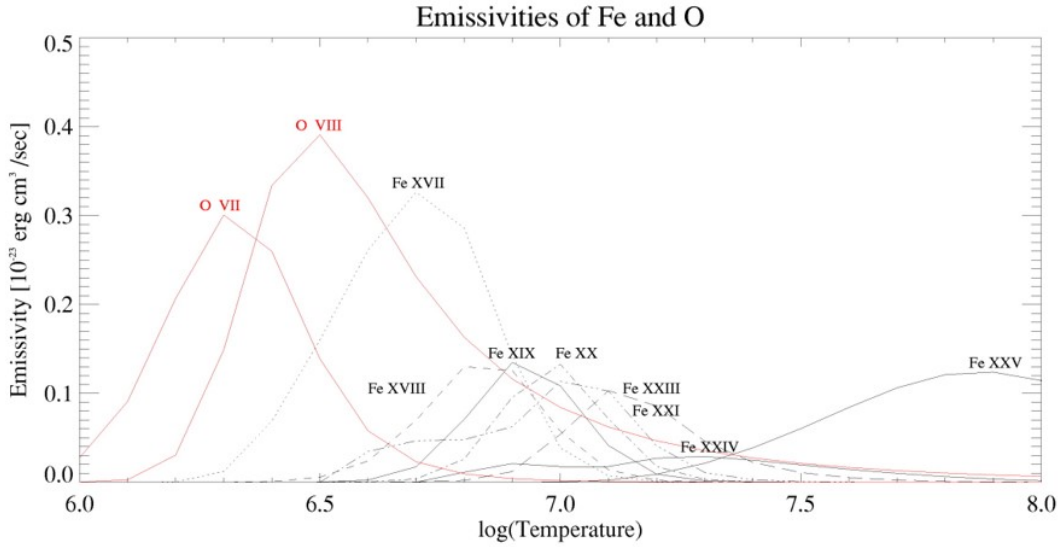

FIGURE 2.3: Emissivity for several stages of ionization of Fe and O (From Telleschi et al., 2005).

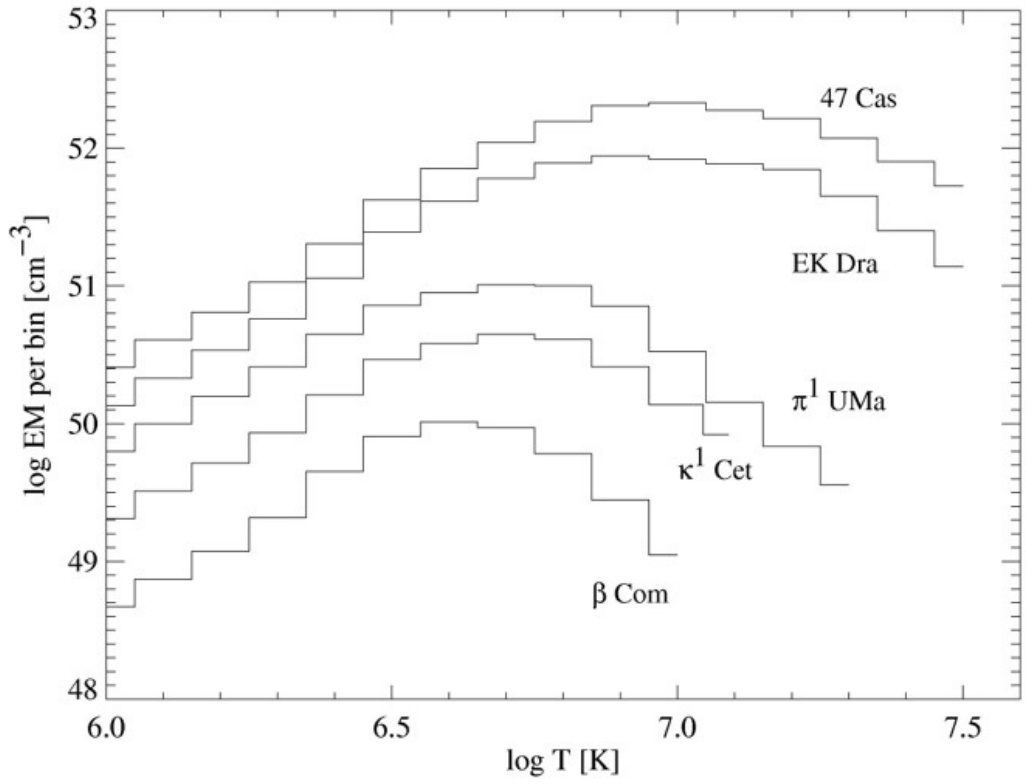

FIGURE 2.4: Emission measure distributions for different solar analogs. (From Telleschi et al., 2005).

2.3 The chromosphere

2.4 Definition of the chromosphere

The following should give a short overview of the solar chromosphere that is based on Hall (2008). For further information the reader might consult this review. Characterizing the other layers of stars above the photosphere is a tedious task, as stars are not static entities, but show variations from short to long timescales. Grossly speaking the chromosphere is above the photosphere, but below the corona with the transition region in between. The chromosphere, as well as the photosphere, is quite a heterogeneous layer that is influenced by magnetic activity. What is seen as dark regions (spots) on the photosphere is seen an bright patches in the chromosphere, usually called “plage", although plage covers a larger area than the associated spots.

Defining what exactly a chromosphere is still has its difficulties. Vernazza, Avrett, and Loeser (1981) have derived a semi-empirical model of the solar chromosphere (Fig. 2.5). Roughly speaking the chromosphere lies in the region between the minimum on the right side of the plot and the sharp increase in temperature that already marks the transition region and corona. Usually, the chromospheric temperature is taken to be some 10 000 K. In comparison, the corona has temperatures of above 1 MK. Hall (2008) uses in his review the following “working” definition for the chromosphere: an excess in emission is observed from what is expected from radiative equilibrium and cooling occurs mostly in strong resonance lines, the most abundant of the lines being Mg II and Ca II. The cooling in the photosphere, on the the other hand, occurs mostly in the continuum.

As we have already mentioned, the chromosphere differs from an atmosphere that is in radiative equilibrium, which means that there are additional radiative losses in some lines, hence those lines are seen in emission. The CaII H&K lines are one prominent example of this process. With those additional radiative losses in some lines, there has to be additional mechanism of heating as well. We have mentioned that magnetic fields and magnetic activity have a large influence on the chromosphere, hence the two most favored theories on chromospheric heating are based on magnetic activity. Babcock (1961)’s model consists of a self-regenerating magnetic field, that is able to explain the main features of visual and magnetic observations of the sunspot cycle. He proposes the heating by Alfvén waves or the transport of mechanical energy along magnetic tubes into the outer layers of the solar atmosphere. On the other hand, Biermann (1948) and Schwarzschild (1948) hold the solar granulation responsible for the heating. The granulation creates acoustic waves that heat the chromosphere, as they develop into shocks and dissipate as they move outwards from the photosphere.

Another interesting question is which stars have chromospheres. As we mentioned before, the chromosphere is not much hotter than the photosphere. This is due to the steadily increasing ionization of hydrogen. The free electrons build up a large pool and can cool the chromosphere due to collisional radiative cooling. The chromosphere is a relatively thick region and the chromosphere can have a large extent. Once the hydrogen is fully ionized, the cooling mechanism does not work anymore and the temperatures rise to a million degrees marking the onset of the corona. With the dissipation of the excess of energy that happens in cool stars through the ionization of hydrogen, one can suspect large extended chromospheres only to be found in cool stars. Moreover, as has been discussed, magnetic field and magnetic activity plays a role in chromospheric activity, which implies the presence of a convective outer layer. Even the non-magnetic

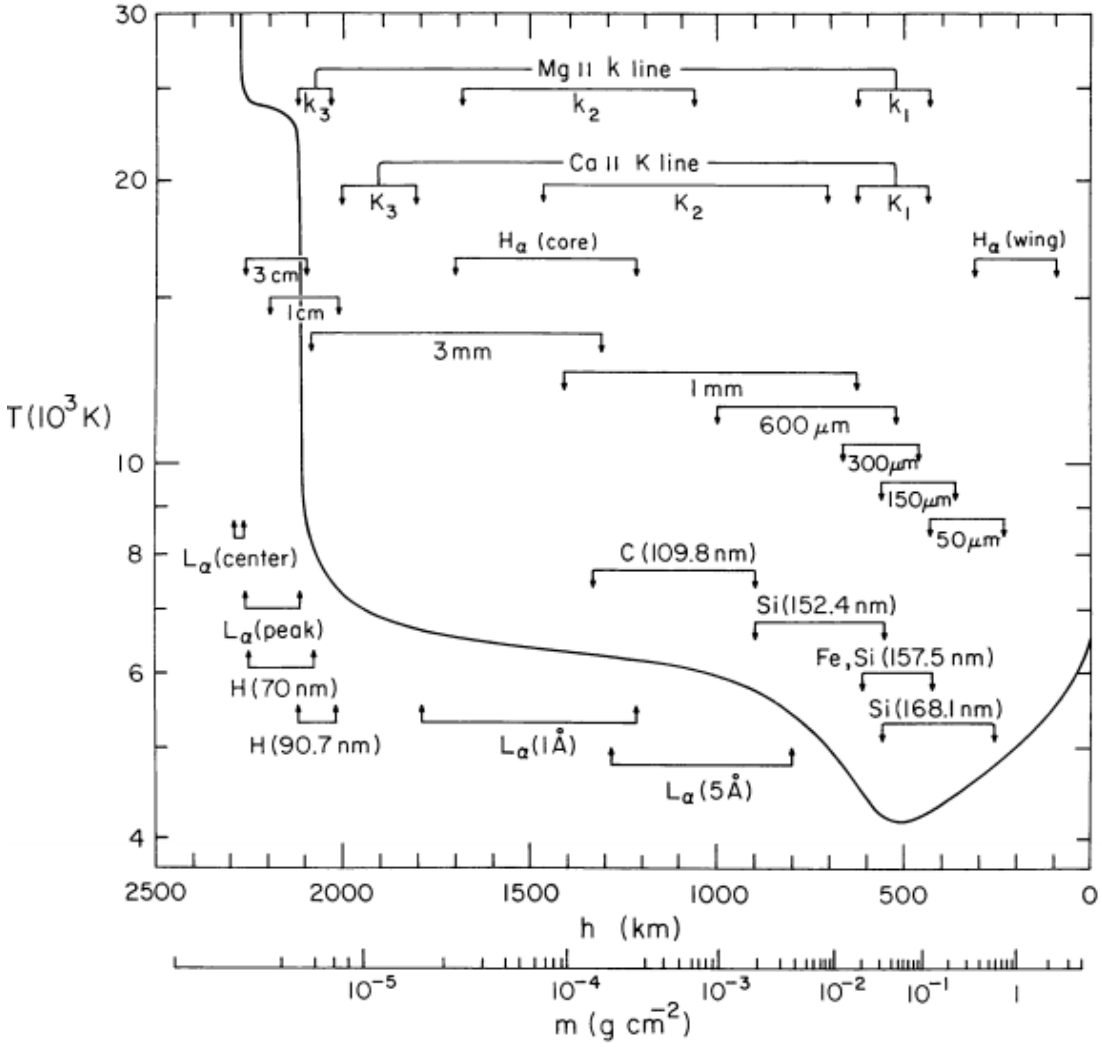

FIGURE 2.5: One of the first chromospheric models by Vernazza, Avrett, and Loeser (1981). The chromosphere spans the region from the dip on the right to the steep increase up to coronal temperatures. The most prominent chromospheric lines Ca II HK, Mg II and H α are indicated as well. (Taken from Vernazza, Avrett, and Loeser, 1981).

sources of energy (e.g. granulation that creates acoustic waves) need a convective envelope. The Sun and solar-like stars have a radiative core and a convective envelope. This inner structure changes as one goes to high-mass stars, with a convective core and a radiative envelope. This transition happens at a stellar mass of approximately 2.3 solar masses.

2.4.1 The S-index and chromospheric activity

Even though the Sun can be resolved as a full disk, it still offers difficulties to mapping for of instance spots, faculae or plage. With other stars appearing as a point source, one has to find other sources of information about stellar activity. One of the most important stellar activity indices is the so-called Mount Wilson S-index (in the following just S-index for short) and is defined as follows,

$$S_{MWO} = \alpha \frac{N_H + N_K}{N_R + N_V} \tag{2.7}$$

with N_H and N_K being the counts in the triangular bandpasses H and K with a FWHM of 1.09 Å centered in the Ca II H+K line cores and N_R and N_V are the counts in the 20 Å continuum band passes R and V centered at 3901.07 Å and 4001.07 Å, respectively (Vaughan, Preston, and Wilson, 1978; Duncan et al., 1991). The factor α is needed, as the Mount Wilson project that started in 1966 (Wilson, 1978) had to undergo a change of the instrument. The advantage of this index is not only the long record, but also that it contains over 100 cool stars in the solar neighborhood, some of them being well studied young solar analogues (Baliunas et al., 1995). Fig.2.6 shows three examples of solar analogues, namely EK Dra (HD 129333), π^1 UMa (HD 72905) and β Com (HD114710) and the Sun. These stars span ages from 0.1- 4.6 Gyr. It is interesting to note, that the S-index decreases with increasing stellar ages. It is also noticeable that the older stars, the Sun and beta Com show a rather cyclic modulation in the S-index, whereas EK Dra and π^1 UMa show no apparent pattern,but the observation time might have been too short for these two stars. For the classification that is given in Fig.2.6 on the top right of the panels, we refer the reader to Baliunas et al. (1995). As the S-index now probes the strengths of the CaII H&K lines, we can also make estimates in the plage coverage of these stars. We will discuss this later in Sec. 4.4.2. For the sake of completeness we also want to mention another index that is related to the CaII H&K lines, namely the so-called R'$_{HK}$ index (Middelkoop, 1982; Noyes et al., 1984). The difference between those two indices is that the R'$_{HK}$ index does not include a colour term and the photospheric contribution to those lines is removed.

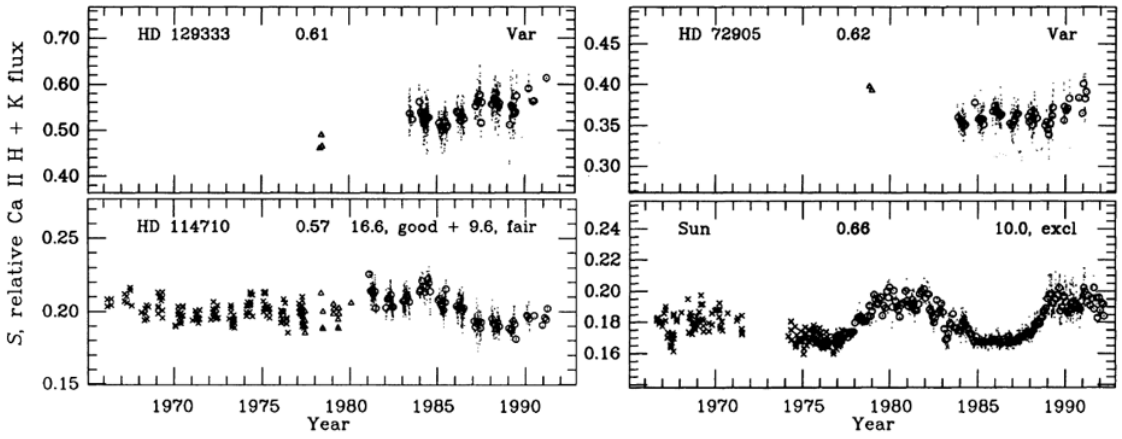

FIGURE 2.6: The S-index for some starve over time from the Mount Wilson Survey. From top left to bottom right: EK Dra, π^1 UMa, β Com and the Sun. (From Baliunas et al., 1995).

Vaughan and Preston (1980) found another interesting phenomenon in the Mount Wilson Observatory Sample, which is the now so-called "Vaughan-Preston" gap. Vaughan and Preston (1980) found this particular feature in the the MWO sample and argued that this gap is a result of a fundamental property of the evolution of the dynamo in cool stars. Several other authors were skeptical of the reality of this gap and it was thought to be a statistical artifact. Noyes et al. (1984) interpreted the gap as a statistical effect that was created by intrinsic upper and lower limits of the S-index arising from photospheric background and chromospheric saturation. However, this gap also appeared in surveys where the R' index (Henry et al., 1996; Gray et al., 2006) and the absolute flux (Hall, Lockwood, and Skiff, 2007) were used, so it appears that the gap is indeed real.

Brandenburg, Saar, and Turpin (1998) and Saar and Brandenburg (1999) found that there is a relation between the ratio of the cycle length,the rotational period and R'_{HK}. Most stars of the MWO survey fall into two distinct parallel samples, an active and an inactive branch. This transition seems to happen at a stellar age of 2-3 Gyr. In the two activity branches two different dynamos seem to be active for the stars, which means that a cool star likely undergoes a drastic change in the dynamo behaviour during its life. The existence of this gap then might be a result of the transition itself that seems to be a fast process. Wilson (1978) already noted that also short-term variations that are related to rotational modulation due to active complexes might be present in this record. Vaughan et al. (1981) found that some late-type stars showing cyclic periods over the time span of years, also show rotational modulation in the S-index with periods measured in days.

We have now established that in the sample of Wilson (1978) different behaviours in the S-index can be seen. We next want to consider the Sun and its cycle before we turn our attention back to solar analogs. Radick et al. (1998) compare the difference in total solar irradiance with the change in S-index. Although the data set is not long, they found that the brightness variation and the variation in the S-index show in-phase behaviour between photospheric activity due to spots and faculae and chromospheric activity in the form of plage and Ca II H&K emission. On the Sun it is clear that spots and plage (or active regions) are clearly correlated. An excess in the chromosphere can already be seen, when no pot is present and as soon as the spot emerges it always will have a chromospheric counterpart. However, it has to be noted that some stars do not show this behaviour. HD 152391 has an average S-index of 0.393 (Baliunas et al., 1995) and a spectral type of G7V (Hoffleit, Saladyga, and Wlasuk, 1983). This is an interesting

phenomenon, as it seems that the star is at its faintest when the S-index is the highest. From the Sun we know on the other hand, that the S-index is the highest, when the Sun is at its brightest. That would mean that on the photosphere spots clearly dominate the emission in this regime for HD 152391, whereas on the Sun the dimming by spots is counterbalanced by a bright feature called "faculae". We will discuss this further in Sec. 3.3.

Chapter 3

Solar and stellar photospheric variability

In Sec.2.2 we have discussed different aspects of coronae and chromospheres of solar type stars. The following is dedicated to discuss our Sun at different wavelengths and look for connections between the outer layers of our central star and the photosphere. Then we will discuss the solar cycle, different ways of modeling solar spectra mostly now concentrated on the visual wavelength regime, before we consider photometric variability of solar-like stars and some methods to determine spot coverages.

3.1 The Sun at different wavelengths

If one was to observe the Sun with a telescope and proper equipment, the observer would either see a plain disk or some dark spots on this disk. These spots are sunspots and appear and disappear in the course of the solar cycle, which we will discuss later in this section. Fig. 3.1 shows a large spot that was observed by NASA's *Solar Dynamics Observatory* (SDO) on 23. Oct. 2014. This spot has a diameter of approximately 128000 km. For comparison: The Earth with a diameter of 12742 km would fit ten times into this spot. The image was taken with the HMI instrument and shows just the intensity of the Sun. It can be seen that the spots consist of two parts: a darker, central region (umbra) and the brighter surrounding called penumbra. The darker colour is a result of a cooler temperature compared to the photosphere. The latter one has an effective temperature of about 5780 K. A spot's penumbra has a temperature range from 5000-5500 K, so is only slightly cooler than the photosphere, whereas the umbra, the core of the spot, lies at about 4000 K.

We now want to compare observations of the Sun in the different wavelengths to highlight the different layers. Fig. 3.2 shows again a coloured intensitygram of the Sun. The reason to show an image similar to that of Fig. 3.1 is that we now want to take a look at some of the Sun's layers with pictures being taken at the same date. In this way, we can be sure that we are able to show the different phenomena on the Sun and their connections through the different layers. Three spots in Fig. 3.2 are seen near the middle and on the left limb of the disk. As the spots are small it is difficult to distinguish between umbra and penumbra on this image.

In white light observations not only the dark spots, but also a brighter feature on the solar photosphere can be seen, namely faculae. Those are features that are also connected to the solar magnetism and are an important feature if one is interested in modeling the solar spectrum in the visual regime or the total solar irradiance (TSI). Faculae can appear without spots, but once spots appear the faculae are enhanced. Fig.3.3 shows the Sun at 1700 Å. The bright patches that are visible are places where bundles of magnetic field lines are concentrated. This shows that faculae are regions of enhanced

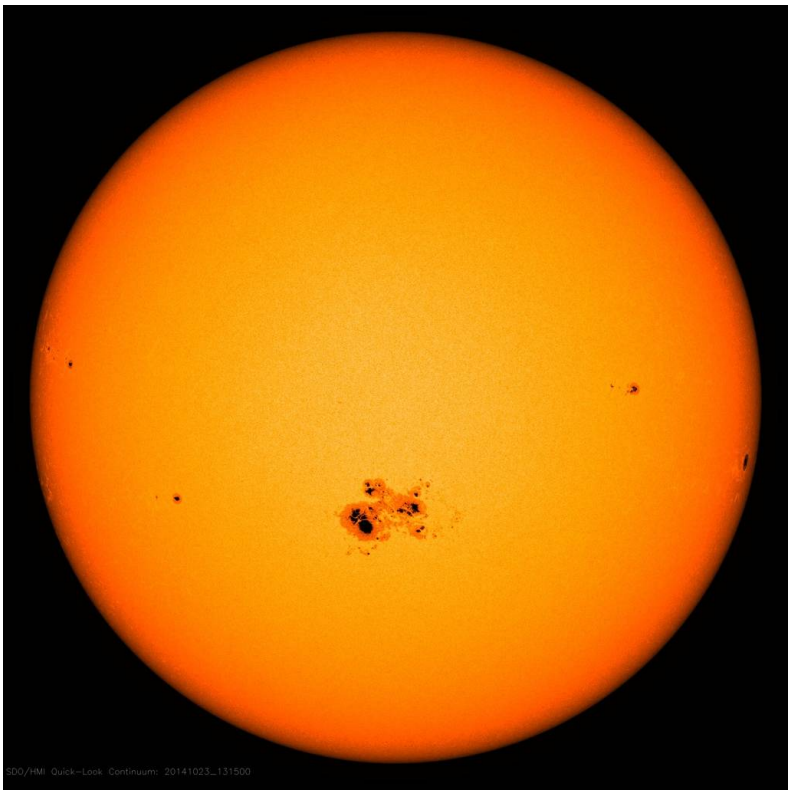

FIGURE 3.1: The biggest sunspot of the current solar cycle observed on Oct. 24., 2014. Image credit: NASA/SDO

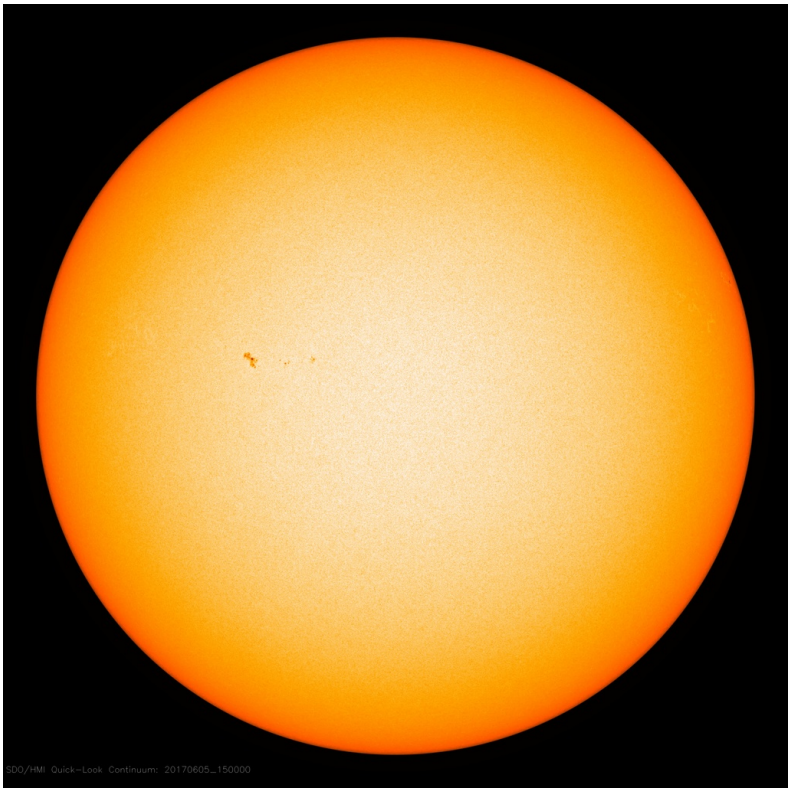

FIGURE 3.2: Sunspots as observed by the SDO on June 5., 2017. Image credit: NASA/SDO

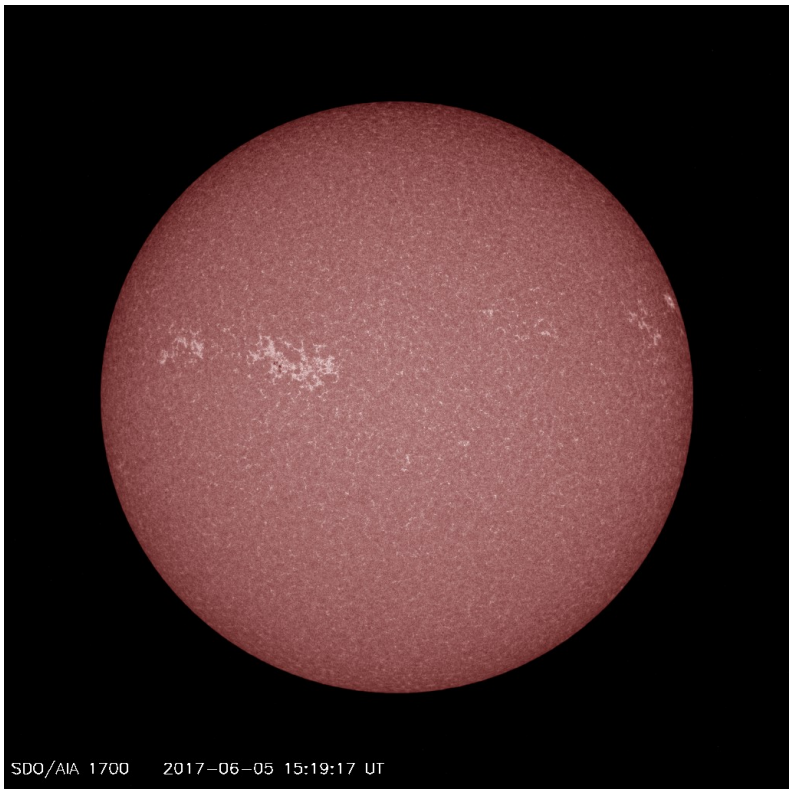

FIGURE 3.3: The Sun seen at 1700 Å on June 5., 2017. Image credit: NASA/SDO

magnetic activity. Compared to Fig. 3.2 the faculae cover more area than the spots, but the spots lie within the brighter faculae features. The small dark dots that can be seen in Fig.3.3 are indeed associated with spots and active regions.

As we will see, the definition of the chromosphere is still a problem in modern solar physics. Its temperatures is higher than the photospheric one, but does not exceed the 1 MK of the corona. Fig. 3.4 shows the Sun through an H α filter at 6562.8 Å. The bright regions are the plage regions. Compared with Fig. 3.3, the two appear on the same place. Note that Fig. 3.4 was not made by the same instrument, neither the same satellite, as the other pictures shown in this section.

The upper part of the solar atmosphere, the corona, is the hottest part with temperatures exceeding 1 MK. The high temperature is reached through the so-called "coronal heating", which is still one of the unsolved problems in solar physics. Fig. 3.5 shows the outmost part of the corona at about 1 MK with the dominant source being FeXII line emission. What was seen as spots and also faculae in the previous regions is seen as bright regions with a lot of coronal loops in this image. With the magnetic field being present, particles are "trapped" and hence show the structure of the field lines. The dark elongated feature is a so-called "coronal hole". In contrast to the rest of the corona, this is a region of lower density. This is because particles that are normally trapped in the magnetic field, can escape along the solar magnetic field from this regions. Coronal holes are associated with fast solar wind. Predicting the occurrence and evolution of coronal holes are therefor an important aspect for space weather research and broadcasting.

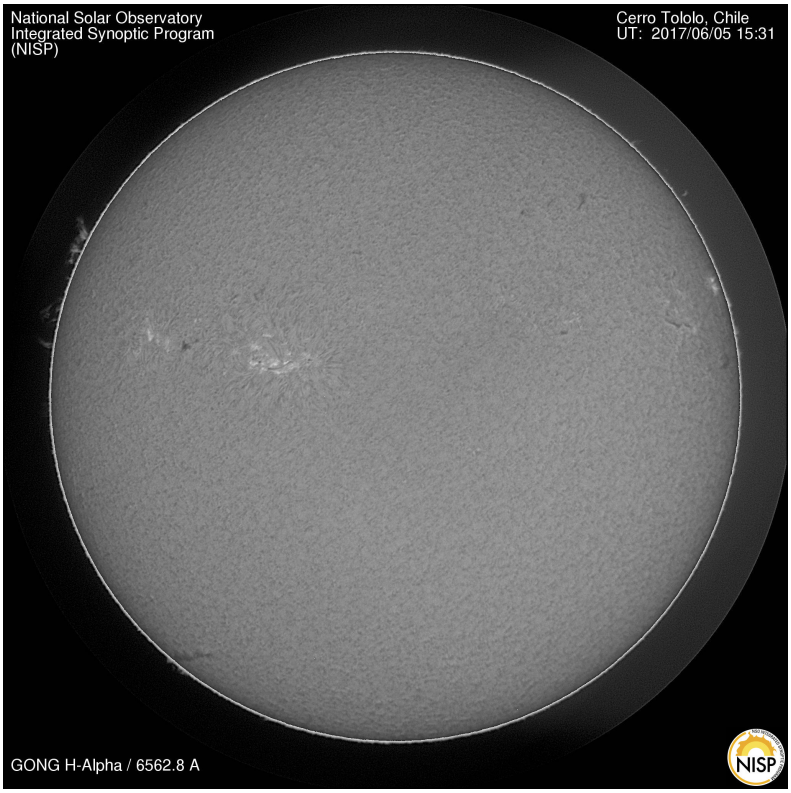

FIGURE 3.4: The Sun seen at 6262.8 Å on June 5., 2017. Image credit: NSO/GONG

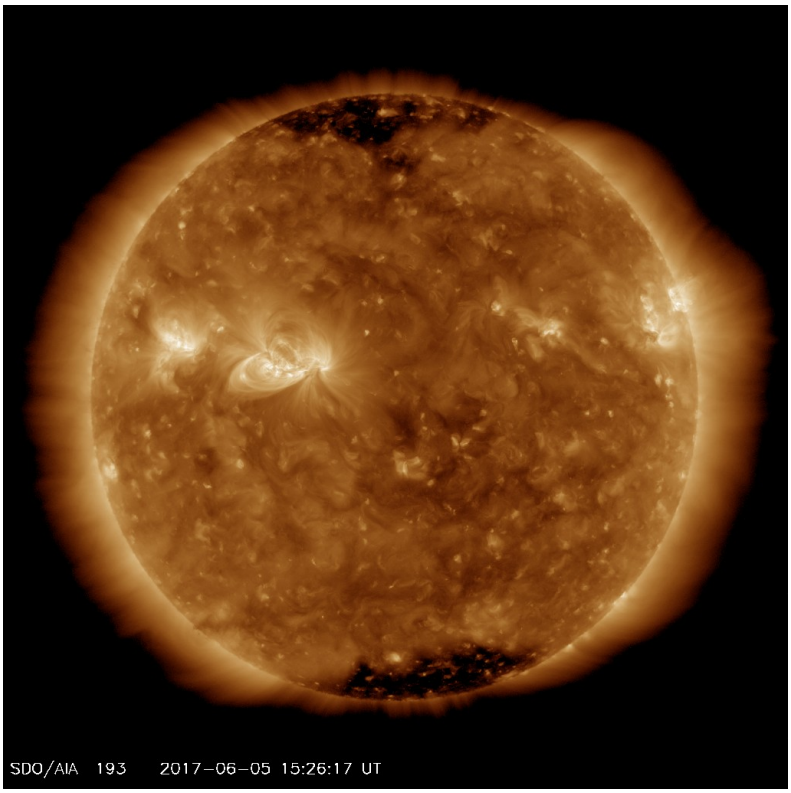

FIGURE 3.5: The Sun seen at 193 Å on March 26., 2017 . Image credit: NASA/SDO

3.2 Solar sunspot and magnetic cycle

A key indicator for solar activity is the number of visible sunspots. At solar maximum there is a high number of sunspots visible on the solar disk, whereas at solar minimum at the end of a cycle there are fewer sunspots to be seen. The sunspot cycle lasts about 11 years (Fig. 3.6), with variations in spot coverage from cycle to cycle. Early observers found that sunspots appear seldom outside a band of 40° centered about the solar equator. Schwabe (1844) was the first to announce this periodicity in the average number of sunspots. A few years later, Wolf (1861) could successfully reconstruct the sunspot number of the cycle between 1755- 1766. This cycle was from then on known as cycle 1. Currently we are in cycle 24, which started around January 2008. Wolf used the following way to calculate the sunspot number

$$r = k(f + 10g) \tag{3.1}$$

where r is the relative sunspot number, g the number of sunspot groups visible on the disk, f represents the number of individual spots (including those distinguishable in groups) and k is a correction factor that depends on the observer (for Wolf: k=1). Today, the International Sunspot Number is used, but other numbers such as the Boulder Sunspot Number exist. Note that the sunspot number is doubted to be the best indicator for the solar activity but is rather used because of its long record. Another way of measuring the solar activity is to look at the Sun in radio at a wavelength of 10.7 cm. This represents the disk integrated solar flux that get enhanced by magnetic activity. The comparative advantage of this method is that the measurements are objective and can be made under all weather conditions. The sunspot cycle has a average length of 11 years, with some variations between 9 and nearly 14 years. Carrington (1858) pointed out that sunspots are observed at latitudes of 40° at the beginning of the cycle.

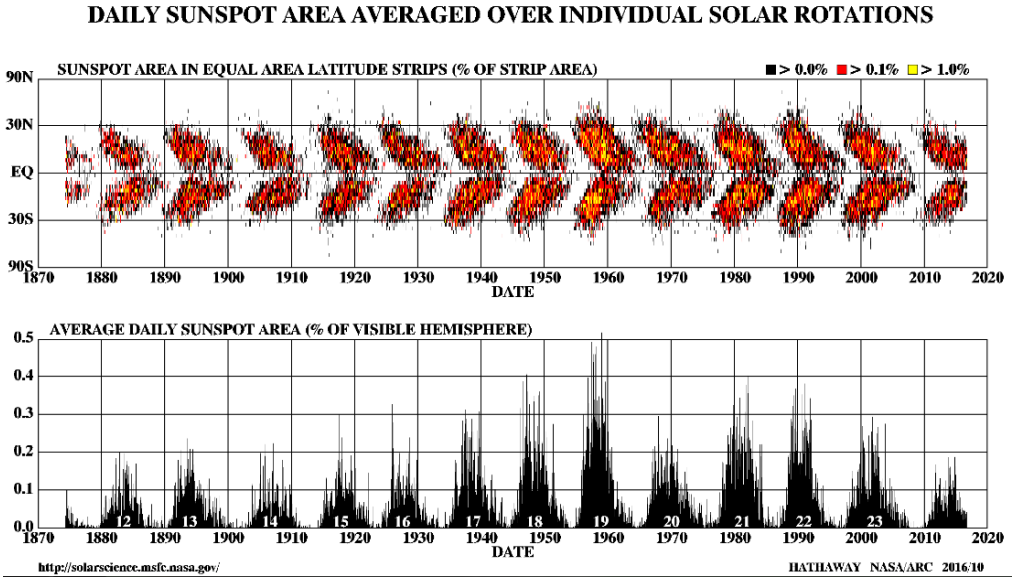

FIGURE 3.6: Top: solar butterfly diagram, bottom: average daily sunspot area. Image credit: David Hathaway/NASA/ARC

As the cycle proceeds sunspots emerge at lower latitudes, until they reach 5°. Fig. 3.6 shows the differences in the cycles and also shows that sunspots are not exactly bound to arise at a maximum of 40°.

Hale et al. (1919) found that large sunspots often appear in pairs of opposite magnetic polarities and established what is nowadays known as Hale's polarity laws applicable at any given time:

- The polarity with respect to the direction of solar rotation of the leading spots of sunspot pairs is the same in a given solar hemisphere.
- The polarity of leading spots is opposite in the north and south hemispheres.
- The sunspot polarities reverse in each hemisphere from one cycle to the next.

The appearance of spot pairs with opposite polarities leads to the following interpretation: What we see is the surface manifestation of a field residing somewhere below the photosphere. This field is known to be a strong small scale field that probably originates somewhere in the tachocline, which is the region between the radiative and convective zone at about 0.7 solar radii. Other than that, a global field is known to exist that is probably a result of the evolution of the fields in active regions. A.H. Joy also found another relation: The line segment joining a sunspot pair shows a systematic tilt angle with respect to East-West direction. The leading sunspot is found to be closer to the equator than the trailing one and this tilt angle increases to higher latitudes. This is known as Joy's law (Hale et al., 1919). Taking a look at Fig. 3.7, a flip in the polarity of the poles can also be seen. Babcock (1959) noted that the pole polarity switches around the maximum of the cycle. In addition to the 11 year cycle, there is as a result a 22 year cycle if the polar field polarity is considered. For further reading on this topic see Charbonneau (2013) and Hathaway (2010).

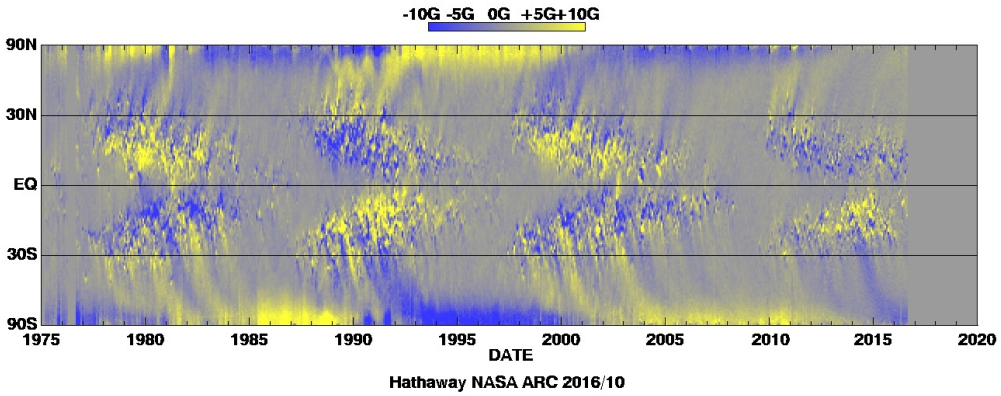

FIGURE 3.7: Magnetic butterfly diagram showing the longitudinally averaged magnetic field strength. Image credit: David Hathaway/NASA/ARC

3.3 Modeling the solar spectrum

Spots are the most dominant feature on the solar photosphere and have an important role on the solar brightness, but not only the spots have an impact on the solar output and its spectrum. As spots are most prominent during the maximum of the 11-year solar cycle, we would expect that at solar maximum the Sun is the dimmest over the cycle. However, this is not the case. The Sun is brightest at solar maximum. This is because faculae, visible as bright patches on the photosphere, weigh out the dimming by spots. If the total solar irradiance (TSI), that is the total integrated flux over the solar spectrum,

is considered the Sun varies by about 0.1 % (**check this number!!**)during it's cycle. The modeling of solar spectra is an important part in solar physics, especially because of its influence on the Earth's climate is so significant. In this section we will now focus mostly on the solar and stellar output in the long-wavelength regime. We discuss the high energy radiation and variability of cool stars in Sect.2.2.

The variation in the solar output has been thought to have an impact on the Earth's climate. Especially the Maunder Minimum (1645 to 1715), that falls into the same time as the small ice age ($\approx$ 1600- 1900) **check this number again!!** is one of the solar cycle extrema that have been observed since the development of the telescope. During this period the sunspot number (or sunspot group number) was low, which suggests that if only the spots are considered to indicate solar activity, the latter one was low at that time. However, also other factors are thought to play a role, as for instance cooling of the Earth due to volcanic eruptions.

Another discussed topic is the solar influence on the Earth's recent climate change, especially the rise in global temperature in the last decades. Solanki and Krivova (2003) have considered three different channels through which the Sun-Earth interaction happens. These are: tropospheric heating caused by changes in the TSI, stratospheric chemistry influenced by changes in the solar UV spectrum and cloud coverage affected by the cosmic ray flux. Earlier works have already shown that since 1970 the secular variations, meaning solar irradiance (Solanki and Fligge, 1998), solar cycle length (Thejll and Lassen, 2000) and solar activity indices (Lean et al., 2001), have decoupled from the evolution of the Earth's global temperature. In Solanki and Krivova (2003) the main assumption was that the Sun has been responsible for the changes in the Earth's global temperature between 1856 and 1970. The year 1970 was chosen as the increase in the global surface temperature since this year has risen by the same amount as in the century prior to this year (Parker, Folland, and Jackson, 1995). The main finding of this study for different channels in the Sun-Earth connection was that even if one considers that the Sun has been responsible for any changes in the Earth's global temperature, the Sun cannot account for more than 50 % of the global temperature rise.

3.4 Stellar variability

Measuring the spot coverage of stars as an activity indicator has its problems, which we want to discuss later in this section. In Sec.2.4.1 we have introduced the S- and R-index as indicators for chromospheric activity. Not only the Ca II H&K lines could be used to measure variability in the chromosphere, but also Hα. On the Sun, we have seen that spots (and faculae) are important for the brightness in the visual wavelength regime. For stars one uses light-curves to understand the brightness variations in different bands. In the 1990's the *Sun in Time* project by Dorren and Guinan (1994b) was initiated. Its goal was to conduct a coordinated multi-wavelength study of nearby, single solar-type stars, combining UV, EUV, X-ray and ground-based photoelectric photometry. These stars have been picked as they are thought to represent the Sun at different ages. In Messina and Guinan (2002) results from photometric studies of BE Cet, κ^1 Cet, π^1 UMa, EK Dra, HN Peg and DX Leo are presented. We use the photometric trends in this work to make an estimate for spot coverages for our sample stars. The ΔV is defined as the difference in the brightest and faintest observed magnitudes and it is used as a measure of spot coverages of a star. However, this is only considered to be a lower limit, as the observed faintest magnitude may not correspond to the actual brightness of a star with no spots. (Neff, O'Neal, and Saar, 1995). This means that even though the star might

seem to be the faintest during a cycle, this might not mean, that there are no spots to be present. Messina, Rodonò, and Guinan (2001) argue on the other hand that with many lightcurves now being available the observed amplitude may reliably approach the actual value.
We want to shortly introduce some techniques to determine spot coverages on stars (other than the Sun) and comment on their problems. Because of these problems with measurements of spot coverages we are using the S-index and the related plage coverage as the building blocks for our spectra. The easiest way to study stellar variability in terms of spots is of course photometry, followed by spectroscopy. For photometry regular observations started in the 1970's and with the help of automatic telescopes, one can observe a large sample of stars regularly. Also space telescope provide long databases with the advantage of not being dependent on the weather or atmospheric conditions. The best known telescopes for this purpose are *COROT*, *Gaia*, *MOST* and of course *Kepler*. Spectroscopy, on the other hand is the most applied tool in astronomy. The study of starspots is based on high resolution spectrographs ($\Delta\lambda/\ \lambda = 500\ 000$) and high-sensitivity detectors, as well as on good time coverage. On the Sun, if the decay of sunspots is now neglected, one would have to observe for ≈ 13 days (rotation period on equator: 24.47 days) to follow the motion of one sunspot across the disk.

Another method, that also requires high time and spatial resolution but probes the stellar magnetic fields directly is polarimetry. This method, however, has unique problems, that we will discussed later. Other methods that we just want to mention for completeness are interferometry and microlensing.

The above observational techniques can help us to verify patterns, but diagnostic techniques have to be used to get for instance spot coverages.

Using photometric data, there are two ways to deduce spot properties. One is direct light-curve modeling (LCM), which is a trial-and-error based method were an assumed number of spots (in a pre-defined pattern and shape) is used to model the observed variations. Numerical methods have been developed and tested by Budding (1977), Vogt (1981), Rodono et al. (1986), Dorren (1987), Strassmeier (1988), Kjurkchieva (1990) and Strassmeier and Bopp (1992) (taking into account the evolution of spots). The second way is light-curve inversion (LCI), where the light curve is inverted back to a spot distribution on the stellar surface. Simply explained, it is assumed that the photosphere consists of two components, namely an hot photosphere and cool spots that are weighted by the factor of their coverage (filling factor). The observed stellar flux is therefore the integrated flux over those two components. As an output of this method one obtains a map of the stellar surface and can deduce spot coverages. Numerical methods have been invented by Messina, Guinan, and Lanza (1998) and Berdyugina, Pelt, and Tuominen (2002). Both LCM and LCI are clearly less informative than techniques that are based on spectroscopy and may only give an lower limit to the spot coverage.

Whereas it is easily evident that spots have an impact on the photometric output of a star, spots also have an impact on spectral lines. This behaviour is used by Doppler Imaging (DI). It does require, as we mentioned before, high-resolution spectral line profiles and rapidly rotating stars. The idea was brought firstly forward by Deutsch (1958) and the first inversion technique with minimization was introduced by Goncharskii et al. (1977). First, this method was used to map chemical peculiarities on Ap stars. For cool stars this method was first used on the RS CVn-type star HR 1099 (Vogt and Penrod, 1983). The star needs to rotate fast enough so that the local line profile is smaller than the rotational broadening of the line. Fig. 3.8 shows the impact on a single spot of a spectral line. It also has to be noted that a spot on the equatorial region has a different

signature in the line than a polar spot. Again, a vital assumption is the nature of the spots in the model calculations as well as the chosen stellar atmosphere model, atomic and molecular line lists and stellar parameters. Small spots that are grouped together are "seen" as one big spot, hence the spot coverage may be overestimated. The advantage of DI is to get temperature maps of stars and to also resolve abundances on the surface.

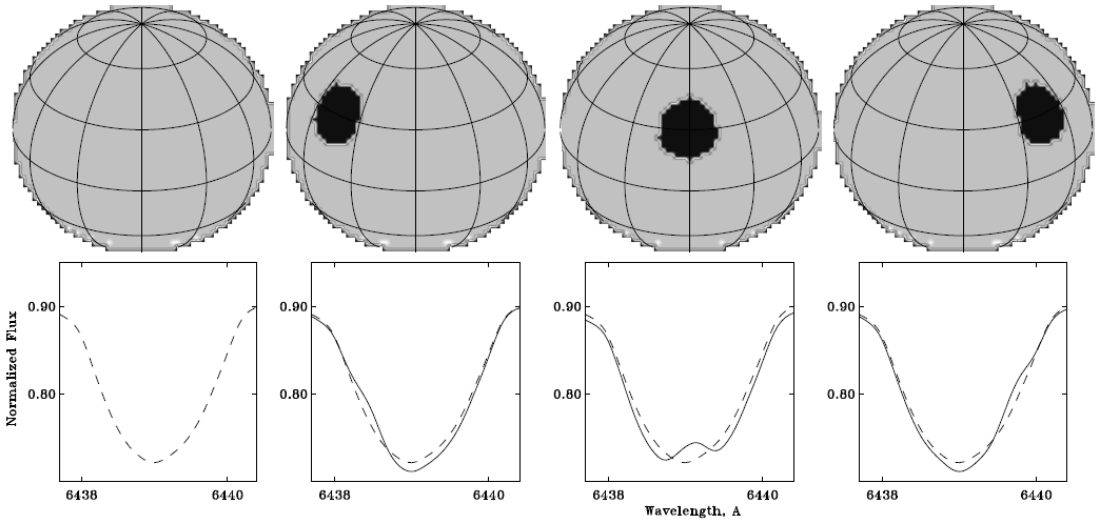

FIGURE 3.8: Spectral line profile for an unspotted star and if a spot moves across a fast rotating star. (Taken from Berdyugina (2005))

Zeeman-Doppler Imaging can be seen as an extension of the classical DI and uses the presence of a stellar magnetic field. Spectral lines are sensitive or insensitive to the magnetic field depending on their Landé-factor. Electromagnetic radiation can be characterized by the Stokes-vector that contains the 4 Stokes parameters I, Q, U and V. I gives the intensity, Q the linear horizontal or vertical polarization, U the linear polarization in $\pm$ 45 $^\circ$ and V the right-hand or left-hand circular polarization. Magnetic fields can split local line profiles (Zeeman-split), the Doppler-shift acts differently on these lines hence the magnetic field distribution can be disentangled. Those splittings are relatively small, so a noise level for Stokes V of 10^{-4} is required. However, the instrumental techniques only allow for a sensitivity that is a factor of 10 higher. Semel (1989) and Semel and Li (1996) suggested using more than one spectral line to increase the signal-to-noise ratio. One of these techniques being Least-Square-Deconvolution (LSD) which allows to gain signal-to-noise ratios of 30 if 200 lines are considered and also lead to mapping of magnetic fields in cool stars (Donati and Brown, 1997). If all Stokes parameters are measured, inversion techniques can be used as well, but measuring Stokes Q and U on stars is difficult, as the magnetic signatures are rather small. Using only Stokes V and I will lead to non-unique results. If all components are measured, the distribution of the magnetic field vectors and the temperature will be retrieved. The inversion also allows to split the magnetic field in radial, azimuthal and meridional magnetic fields. Fig. 3.9 (from Rosén, Kochukhov, and Wade, 2015) shows the difference in the magnetic field distribution on the surface and the extrapolation of the field lines. We clearly, that using only I and V, the solution is fairly different from one using all four Stokes parameters.

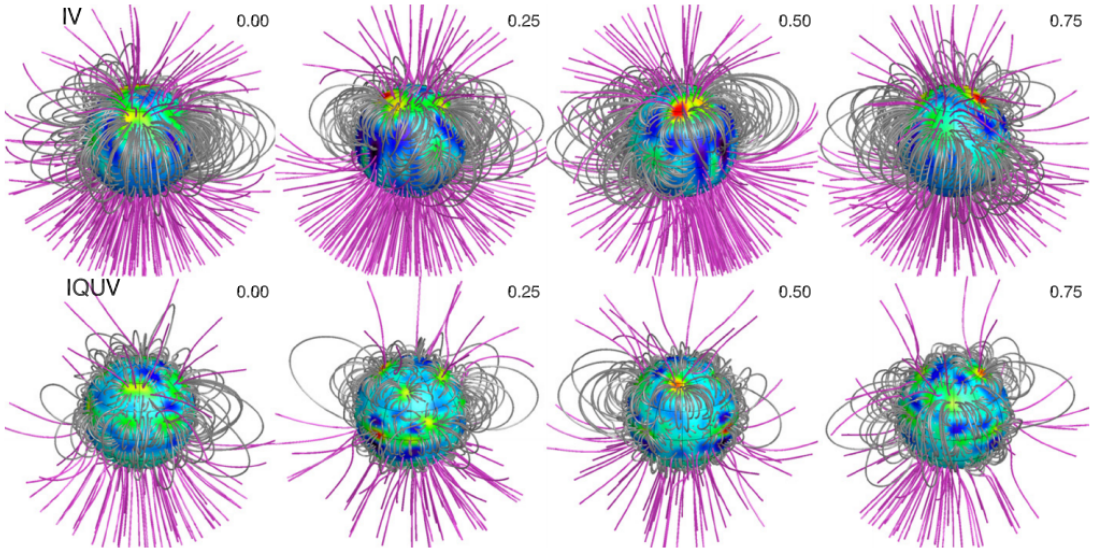

FIGURE 3.9: Spot distribution on II Peg. Top row was obtained by using a magnetic field extrapolation using Stokes V and I. The bottom row was obtained using all Stokes parameters. (Taken from Rosén, Kochukhov, and Wade, 2015)

For the sake of completeness, we also want to mention the possibility of molecular band modeling (MBM), using line depth ratios and even asteroseismology as a diagnosis for stellar magnetic fields. For further reading see Berdyugina (2005).

All above mentioned techniques have their drawbacks and a major problem is that different techniques yield different results. If for instance spectropolarimetry is chosen, the results will depend on the inversion technique. Even if a map of spot distribution is available, it is difficult to constrain the area coverage of spots, as this depends on different parameters such as temperature. We show the difference in measurements from various techniques on the example of EK Dra in Tab.3.1. It is clearly evident that for every method a different spot filling factor was retrieved. With the values for the spot temperature T_{spot} being different and even a different effective temperature being chosen, it is hard to find definitive results for the "true" spot coverage for each star. The filling factor obtained with LCM is likely to be a lower limit, the value from DI being a bit more reliable and still reasonable, but the spot filling factor obtained with MDM should be seen as an upper limit. We have discussed earlier in this section the findings from Messina and Guinan (2002), which are of photometric nature. In order to make use of the knowledge in difference of ΔV in stars, we decided to use a spot coverage of EK of 6 % for our purpose. We will discuss in Sec. 4.4.2 and in Sec. 5.6 the effect of choosing the "wrong" spot coverage.

Method	T_{eff} [K]	filling factor [%]	T_{spot} [K]	Reference
LCM	5930	6 (s)	5400	Dorren and Guinan, 1994a
DI	5850	11(d)	4800	Strassmeier and Rice, 1998
MBM	5830	40 (d)	40	O'Neal et al., 2004

TABLE 3.1: Different spot coverages for EK Dra obtained with three different methods. The filling factor is either normalized to the whole stellar surface (s) or to the stellar disk (d)

With the above mentioned issues of using the spot coverage as an input for our model, we decided to use the S-index (see Sec. 2.4.1) as the best-suited and least biased activity indicator and input for our models. There is, however, still the issue of converting the S-index into a area coverage of plage, but in Sec. 4.4.2 we will address and partially solve this issue.

Chapter 4

Models for solar and stellar EUV

4.1 Modeling of the transition region

Juan Fontenla and his collaborators have been working on modeling the solar spectra since the 1990s. We now want to give a short overview of the work that has been done leading to the development of the spectra used in the present work.

Fontenla, Avrett, and Loeser (1990) is the first paper in a series that deals with the different layers of the solar outer atmosphere. In this paper the was the analysis of the energy balance in the lower transition region. The transition region is the layer between the chromosphere and the corona. In this particular layer several properties change, one important being that the chromosphere is opaque, chromospheric lines are optically thick. Also the ionization of hydrogen plays in important role as has been discussed in Sec.2.3.

The most prominent problem that come with modeling the transition region are that a range of temperatures are present. They are going up to nearly coronal temperatures, but also down to photospheric temperatures. Emission measure modeling that can be done for the corona does not work anymore, once the temperatures are below 1 MK. This problem arises because the lines are optically thick. This paper treats the modeling based on the following simplifications: to avoid complex geometry a plane parallel stratification is assumed and effects of the magnetic field in the transport coefficients are neglected. However, radiative losses are computed using the detailed solution of the statistical equilibrium and the radiative transfer equation for hydrogen. Ambipolar diffusion is included, mass motions are neglected. The work concluded with the findings that a reasonable energy balance model can be constructed for the Sun's lower transition region even though simplifications were made. The authors state that it was not intended to match any observations with this work, but rather to introduce this new model.

Fontenla, Avrett, and Loeser (1991) presented several improvements and also the building blocks of the spectra used in our work are presented. The calculated spectra that correspond to various solar features such as faint-cell center areas (A), average intensity areas (C), bright network regions (F) and plage area (P) (the components are discussed in detail later). The main findings of this paper were that hydrostatic models of the solar atmosphere are able to explain a number of observations. This work also used an update of spectra that were already present in the work by Vernazza, Avrett, and Loeser (1981), the so-called VAL models. The lines present were still only Lyman-α and Lyman-β, so further elements were to be added.

Fontenla, Avrett, and Loeser (1993) added helium into their calculations and were able to explain the observed intensities and profiles at the He I resonance line at 584

Å, which other models could not do. Still the model is a 1D hydrostatic model with a plane-parallel atmosphere in hydrostatic equilibrium having a distribution in temperature. The energy that is radiated is balanced by a particle down-flow from the corona. The new feature in this work is, that helium diffusion was carried out in non-LTE radiative transfer and in the statistical equilibrium calculations. Generally the observed EUV line profiles and intensities were found to match observations.

This series of papers was concluded by Fontenla, Avrett, and Loeser (2002) with the addition of particle and mass flows, that are quasi-steady and satisfy the momentum and energy balance equations in the transition region. The models were again in simple 1D geometry and included flow velocity terms in all equations while neglecting terms with time derivatives. All calculations were done using non-LTE modeling. The models presented in all four papers are able to fully selfconsistently treat the radiative transfer equation, plus the statistical equilibrium and the energy and momentum balance, including detailed calculations for H and He. The FAL models now included still "only" 4 different features of the Sun, but it was already shown that these features play an important role in modeling the solar spectra.

4.2 Semi-empirical models

After the first findings, a second series of paper was published adressing the semi-empirical modeling of the solar atmosphere. Fontenla et al. (2006) constructed models for the quiet and active Sun at moderate spatial and temporal resolution (3" and $\approx$ 30 min, respectively). Only hydrogen is treated in full NLTE, the other lines were calculated using approximate NLTE. In this paper only the photosphere was modeled, hence the spectra calculated were able to reasonably reproduce the solar spectrum in the visual and infrared wavelength regime, but not at the short wavelengths. Nevertheless, we will discuss the features presented in this model in more detail, as some of them are also present in the input for our models. The FAL model C is, as has been discussed earlier, a modification from Vernazza, Avrett, and Loeser, 1981 (VAL C) and is described as the area that has the same intensity as the median in a histogram of Ca II K image of a quiet area of the Sun. This model hence is an average, quiet Sun. As mostly super-granular cells are seen here, this model is called "quiet Sun cell interior". Model E (also VAL-E) is the bright area between super-granular cells and is the so-called "quiet Sun network". Model F (VAL-F) are network lanes that are brighter than the average and represent the "active network". Models C and E are not related to solar activity, but there is a correlation between the brightness and the magnetic field in the quiet Sun network. Fontenla et al. (2006) also added new features, which represent the active Sun. The sunspot penumbra (R) and umbra (S) models are both taken to be an average penumbra and umbra at a moderate resolution and were identified using the Precision Solar Photometric Telescope (PSPT) red band data (white light). With this data also faculae (P) have been identified. Note that here the definition changed from the 1991- models. The plage area (H) has been found in filtergram taken in Hα and CaII K. Fontenla et al. (2006) describe faculae as part of active regions that are brighter than the quiet Sun at red continuum wavelengths at disk positions μ<0.5, and plage as parts that are visible in chromospheric lines, e.g. in the K_3 and K_2 features of the Ca II line, but are not visible in red continuum. To summarize: the FAL models now include 7 solar features only in the visual and infrared wavelengths.

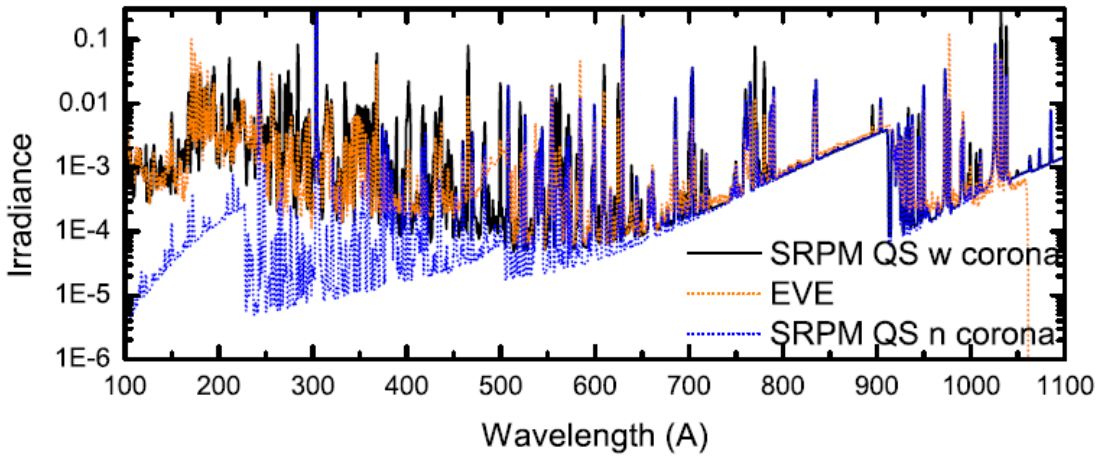

FIGURE 4.1: Modeled spectra (blue and black) compared to measurements from the Extreme Ultraviolet Variability Experiment (EVE) onboard of SDO (orange) during solar minimum. Note the difference if one includes the corona in the models. The black line includes the corona and matched the observations fairly well, whereas the spectrum in blue (without corona) fails to reproduce the spectrum below 600 Å. The irradiance is given in erg s^{-1} cm^{-2} $Å^{-1}$. (From Fontenla et al., 2009)

Fontenla et al. (2009) includes the upper chromosphere and transition region to extend the models to the FUV and EUV. Small changes have been made to the 2006 models to better match observations in the visual and IR regime, but the chromosphere and transition region have been significantly changed to match observations by SOHO/SUMER. The names of the models and the components have changed a bit again. In order not to confuse the reader more with definitions and letters, we refer to the list at the end of this chapter, where the abbreviations and definitions of the components are given. Fig. 4.1 shows that part of the EUV radiation also comes from the corona, so a proper description of the corona, chromosphere and the transition region are needed to match observations in the EUV. Especially below 600 Å the coronal emission dominates the spectrum.

Fontenla et al. (2014) present all 9 models that are used in the present work. Table 2 in this paper gives all elements for which full NLTE radiative transfer was included. Whereas in the previous papers full NLTE was computed only for hydrogen, the models include now nearly 40 species, including also singly and doubly ionized atoms such as Ca II or N III. This paper also presents 6 days for which the solar spectrum was reconstructed in the following way: all components were multiplied by a weighting factor (filling factor) depending on the coverage of the respective components. These weighted components were then added to result in the synthetic solar spectrum for a given day.

In Fontenla et al. (2011) components A and B and P and Q were added. Note that a filling factor of for instance 0.5 means 50 % coverage of the solar disk with this particular feature. Fig. 4.4, 4.5, 4.6 (provided by J. Fontenla, private communication) show all components present in the list above. These spectra have the corona from Fontenla et al. (2014) with the Fontenla, Stancil, and Landi (2015) chromosphere with a slightly modified transition region. We here only show the EUV part from 360-920 Å, but the full given spectra span from 0.22 to 1600 Å.

4.3 Ways of modeling stellar EUV

Fontenla and his collaborators are able to model the Sun self-consistently from the XUV down to the infrared. Other works have been published that are able to model the solar spectrum as well, all based on the magnetic features on the Sun, but mostly just the visual wavelength regime is considered. Compared to the flux in this regime, the XUV flux is small, nevertheless, it has an huge impact on surrounding planets. The following should give a short overview of other works that had the goal to model the “missing" flux in the 36-92 nm regime for other stars than the Sun. Due to interstellar extinction it is not possible to measure in the mentioned regime.

The paper that sparked the idea for the present work was Ribas et al. (2005) on the Sun in Time sample. This paper describes six solar analogues, with one being older and five being younger than the Sun. These stars are EK Dra, π^1UMa, χ^1 Ori, κ^1 Cet, β Com and β Hyi. The ages in this sample range from 0.1 Gyr for EK Dra to 6.7 Gyr for β Hyi. The effective temperature for this sample is solar like, with the exception of β Com, which has an effective temperature of 6000 K. The young solar analogues all have a slightly lesser mass than the Sun and also their radii are a bit smaller than the solar radius. All of these stars are well studied and build the basis for several samples of young solar analogues. Ribas et al. (2005) shows the problem for the modeling of the EUV, as measurements are not possible between 360 and 920 Å due to interstellar extinction. In this paper three approaches for solving this problem are mentioned, namely (1) the use of empirical irradiance from the Sun with scaling relations to account for higher activity, (2) extrapolating between measurements of the EUVE satellite and the UV or (3) compare the flux evolution in other wavelength ranges and derive the total missing flux in this particular wavelength regime by interpolation. Ribas et al. (2005) decided to use the third approach. With this they were able to give the results presented in Table 4 in their work. Fig. 4.2 (Fig. 7 in Ribas et al., 2005) show the flux density from the X-rays to the UV for the stars in this sample. The trend clearly shows that the spectra become less intensive with age, but the whole spectrum does not decay by constant factors across the wavelength range.

Sanz-Forcada et al. (2011) used a coronal model to synthesize the spectral energy distribution (SED) in the whole EUV range. For this one has to know how the plasma is distributed with the temperature in the corona and the transition region. This emission measure distribution (EMD) from the corona is then folded with an atomic model. In this case the APEC model (Smith et al., 2001) was used. Chadney et al. (2014) used these models to construct XUV spectra for ϵ Eridani, AD Leonis and AU Microscopii. ϵ Eridani is a K dwarf and AD Leonis and AU Microscopii are M dwarfs. In this work the constructed spectra are shown in comparison with a solar spectrum and scaled solar spectra. The scaling of solar spectra are another way of constructing stellar spectra in the EUV range. However, Chadney et al. (2014) show that a scaling with two parameters, meaning two factors with which the solar spectrum is multiplied, is better than with just one parameter, but still the stellar spectrum cannot be fully matched, though the shape of the spectra obtained with the scaled-up solar spectra is quite well resembling the one from the modeling.

4.4 Our approach

As we have discussed different approaches to model the Sun and more active stars in this chapter, we now want to conclude with presenting our approach. Fontenla et al.

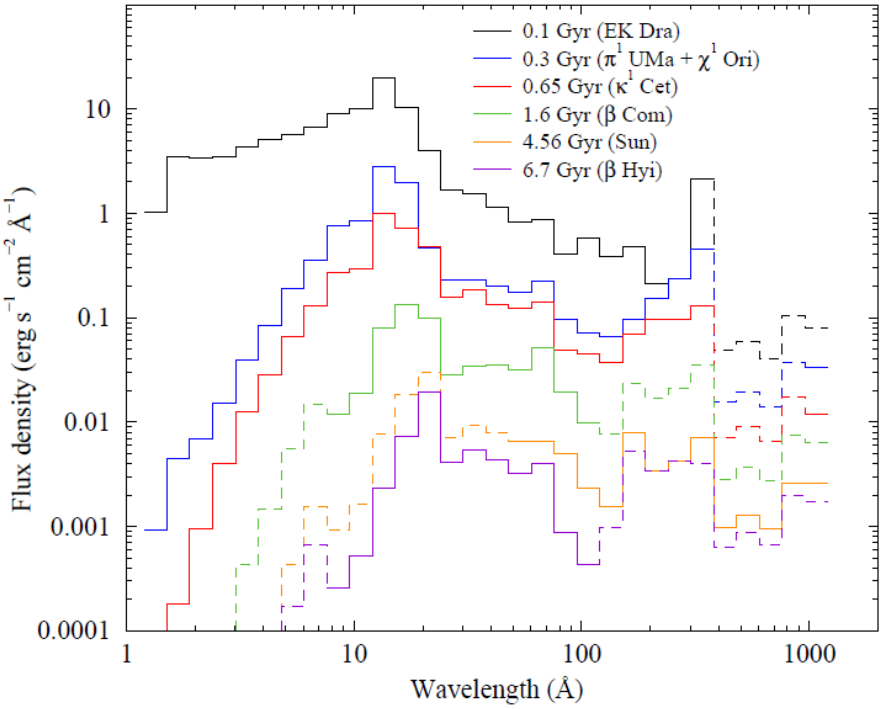

FIGURE 4.2: Spectral energy distribution for the Sun in time sample in Ribas et al. (2005). Taken from Ribas et al. (2005)

(2009) have shown that it is possible to model the solar irradiance by weighting and co-adding different features of the Sun. In general, it should be possible to construct a general trend for more active stars than the Sun with the component spectra using different weighting factors. For the Sun the spot coverage is often used as an input for calculating solar spectra. On stars with the problem that comes along with measuring spot coverage (see Sec. 3.4), we decided to use the S-index (see Sec. 2.4.1) as an activity indicator. This index is related to the plage coverage and gives therefore information about the chromospheric activity. We then scale all other features relative to the plage coverage. The big advantage of this approach is that we are able to obtain a good and quick estimate of fluxes in the desired wavelength regime (in our case 360-920 Å) for any star with a given S-index (or R' index). Baliunas et al. (1995) present S-indices for hundred stars including $\approx$ 20 G-type stars, including all well-known young solar analogues.

4.4.1 Description of the solar spectral features

The following list gives the abbreviations and short descriptions of the solar features as given in Fontenla et al. (2011).

- Dark-quiet-Sun inter-network (A)
- Quiet-Sun inter-network (B)
- Quiet-Sun network lane (D)
- Enhanced network (F)
- Plage (H)
- Facula (P)

- Sunspot Umbra (S)
- Sunspot Penumbra (R)
- Hot Facula (Q)

We now take a closer look of all components from the list above and present their scaling relations.

Spots

Sunspots have proven to come in different shapes (e.g. Strassmeier, 2009), however we do not want and do not have to distinguish between different shapes. Spots and their evolution are important for understanding the magnetic dynamo. These features show strong magnetic fields. Hathaway (2013) gives a good review on this topic. Sunspots are made of two parts: umbra (S) and penumbra (P). Hathaway shows that the ratio of P to S goes from 5 to 6 as the spot varies from 100 to 2000 micro-Hemispheres. We decided to use a ratio of 6 as this may work better for large spot coverage. Temperature and brightness mapping cannot yet resolve the two components, which is another problem and reason not to use the spot coverage as the starting point for our model.

Faculae and Plage

Faculae (Latin; torches) and plage (french; beach) have shown to be particularly tricky but important. Most literature defines plage as an area with enhanced brightness due to emissions, that can be seen in H α and Ca II H&K lines (emission lines). Physically, plage are regions of enhanced temperature and density in the chromosphere heated by magnetic fields. Plage cover usually most areas of the active regions. Active regions are regions in the chromosphere that mostly map the underlying sunspots in the photosphere but are more extended. Plage can exist before and after the emergence of sunspots, but whenever there are spots, they are surrounded by plage.

Faculae and plage can be seen as the same phenomenon, but faculae reside in the photosphere and can be seen in white-light only near the limb. Faculae can exist without spots, and with spots they are enhanced. During solar maximum, with a high coverage of the Sun with spots, it is the faculae that balance the dimming of the light resulting from spots. Foukal (1993) analyzed data from the Royal Greenwich Observatory (RGO) from 1874-1976 covering cycles 12-20. In a follow-up paper plage coverage from cycles 16 to 20 are presented in daily and annual averages Foukal (1998) . The lifetime of plage and spots plays an important role. It is suggested that plage and facula have longer lifetimes than spots. We use the daily averaged data as it represents snapshots of the Sun and we are more interested in these than the time evolution of the components (see Fig.3.6). We find that cycle 19 in Foukal (1998) is the most active recorded cycle for the Sun and use this as a starting point for further investigations.

Finding scaling relations for the faculae to spot coverage has proven to be difficult. Foukal (1998) also gives values for the faculae coverage, however here the RGO data does have several drawbacks. The biggest one is that the white light faculae can only be seen at the limb, where the contrast is the highest.

Here the table given by Fontenla et al. (2011) matters. This table gives filling factors for six days of solar cycle 23, from which filling factors were derived for the different components. In order to do so magnetograms from PSPT were used. Another issue is that in this work the sum of facula (P) and hot facula (Q) is used. The hot faculae

show a higher intensity in the spectrum than the "normal" facula (Fig.4.5) The reason to go with Fontenla et al. (2011)'s sum of the components is that we cannot distinguish between faculae or hot faculae on other stars than the Sun. Secondly, the fraction of P+Q rises with increasing plage and spot coverage, which makes sense if all features are seen as results from magnetic activity. We do not see a reason why faculae should decrease with increasing spot coverage, but have to keep at least in mind, that there might be a saturation.

Enhanced network

Enhanced network is seen mostly in the boundaries between granules and it is stronger with higher spot coverage. The enhanced network from Fontenla et al. (2011) scales fairly well with plage. The ratio between enhanced network and plage is 2.5 with a deviation of 0.67.

Quiet Sun

Fontenla et al. (2011) add components A and B. It seems that the sum of these two scale well with component D (Quiet-Sun inter-network lane) with a ratio of 4.06 and a deviation of 0.2. For our sample, the quiet regions do not play any role. We mostly focus on spot, plage and faculae and fill up the rest of the surface with the next features of lower intensity, so in our case the enhanced network.

4.4.2 Scaling relations

We have discussed the S-index in Sec. 2.4.1 and decided for it as our principal activity indicator and starting point for our scaling relations. Shapiro et al. (2014) have shown the the solar S-index is correlated with the plage coverage via

$$A_H(S) = -0.233 + 1.4 \cdot S_{MWO} \tag{4.1}$$

where S_{MWO} is the S-index and A_H is the area plage coverage. Here again one has to be careful with definitions. Shapiro (priv. comm.) considers plage and faculae to be the same phenomenon that is just seen in different layers of the solar atmosphere. With any given S-index we are now able to derive a plage coverage for any star.

Establishing a relationship between plage and spot area has proven to be a difficult task. We use the average S-index from Baliunas et al. (1995), so as a result we get an average plage index and now have to derive the average spot coverage. As we will show later in the desired wavelength regimes between 36-92 and 92-118 nm plage, faculae and the two spot components are in the same order of magnitude of flux. However, as we will show, the plage coverage will dominate the spectrum. An error in the spot coverage, does not have an huge impact on the resulting fluxes and spectra. Dorren and Guinan (1994b) have used lightcurves of EK Dra and found a lower limit for the spot coverage of 6 %. Messina and Guinan (2002) show the relation between the difference in brightest and faintest magnitude and the inverse Rossby number. We have extracted the data and present in Table 4.1 ΔV for some stars. If we consider that the change in brightness is only caused by spots, we can compare these values for different stars. With the spot coverage for EK Dra, we can also get a rough estimate of spot filling factors for the other stars. We again emphasize that these values will likely be only lower limits. Fig. 4.1 shows solar cycle 19 with the added values for some stars that are presented in Tab.4.1. As we have discussed in Sec. 3.4, we used the difference in photometric variability of

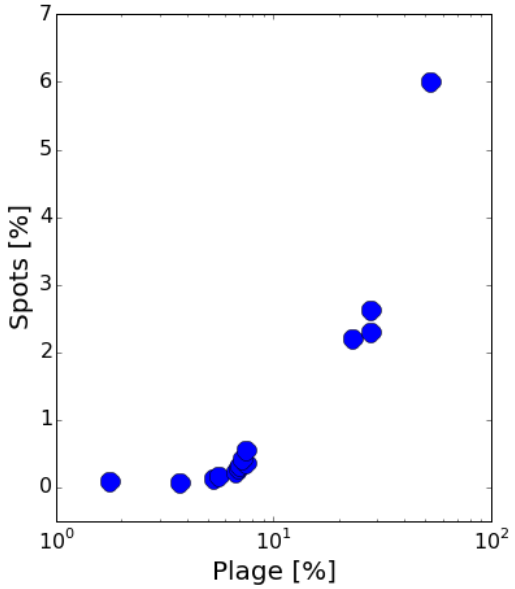

FIGURE 4.3: Plage vs. spot coverage for solar cycles 19 and the values in Tab. 4.1. Data for the solar cycles was retrieved from Foukal (1998), the photometric differences from Messina and Guinan (2002).

Star	ΔV	Ratio	Spot coverage [%]
EK Dra	0,18	1	6
π^1 UMa	0,079	2,28	3
κ^1 Cet	0,069	2,61	2
HN Peg	0,066	2,73	2

TABLE 4.1: Photometric variability and the resulting spot coverage in comparison to EK Dra. ΔV was retrieved from Messina and Guinan (2002). "Ratio" denotes the difference between the stars and EK Dra in terms of ΔV.

stars and EK Dra and the derived spot coverage for EK Dra to get an estimate of spot coverages for 2 more stars. The values in Tab. 4.1 were rounded as to a precision of 1%.

We find that with cycle 19 and our additional stars that plage and spots (here taken to be the sum of umbra and penumbra) show the following relation:

$$A_{R+S} = 0.00041 \cdot A_H^2 + 0.098 \cdot A_H - 0.32 \tag{4.2}$$

The two components R and S of spots are taken to have a constant ratio (given by Hathaway, 2013);

$$\frac{R}{S} = 6 \tag{4.3}$$

The next spectral component that is of interest is faculae. The spectra we were given by Juan Fontenla have faculae (P) and hot faculae (Q). Both differ only in their brightness compared to the quiet Sun. Note that usually only one species of faculae is considered. From Fontenla et al. (2011) we find that

$$A_{P+Q} = 4.31 \cdot A_H^2 - 0.13 \cdot A_H + 0.0023 \tag{4.4}$$

The next component can also be counted as an "active" Sun feature, namely feature F or enhanced network. Again, in Fontenla et al. (2011), we find that the enhanced network stays almost proportional with plage,

$$A_F = A_H \cdot 2.5 \tag{4.5}$$

We are now left with the quiet Sun components. For more active stars we expect that their role is either small or non-existent. Given the values for the filling factors in Fontenla et al. (2011) we find Eq.4.6

$$A_{A+B} = A_D \cdot 4.06 \tag{4.6}$$

In practice, we first put plage on the star, add faculae and spots, then the enhanced network. The rest is then filled up with the quiet Sun components.

For a better overview we summarize all equations again;

$$\begin{aligned} A_H(S) &= -0.233 + 1.4 \cdot S_{MWO} \\ \frac{R}{S} &= 6 \\ A_{R+S} &= 0.00041 \cdot A_H^2 + 0.098 \cdot A_H 0 - 0.32 \\ A_{P+Q} &= 4.31 \cdot A_H^2 - 0.13 \cdot A_H + 0.0023 \\ A_F &= A_H \cdot 2.5 \\ A_{A+B} &= A_D \cdot 4.06 \end{aligned}$$

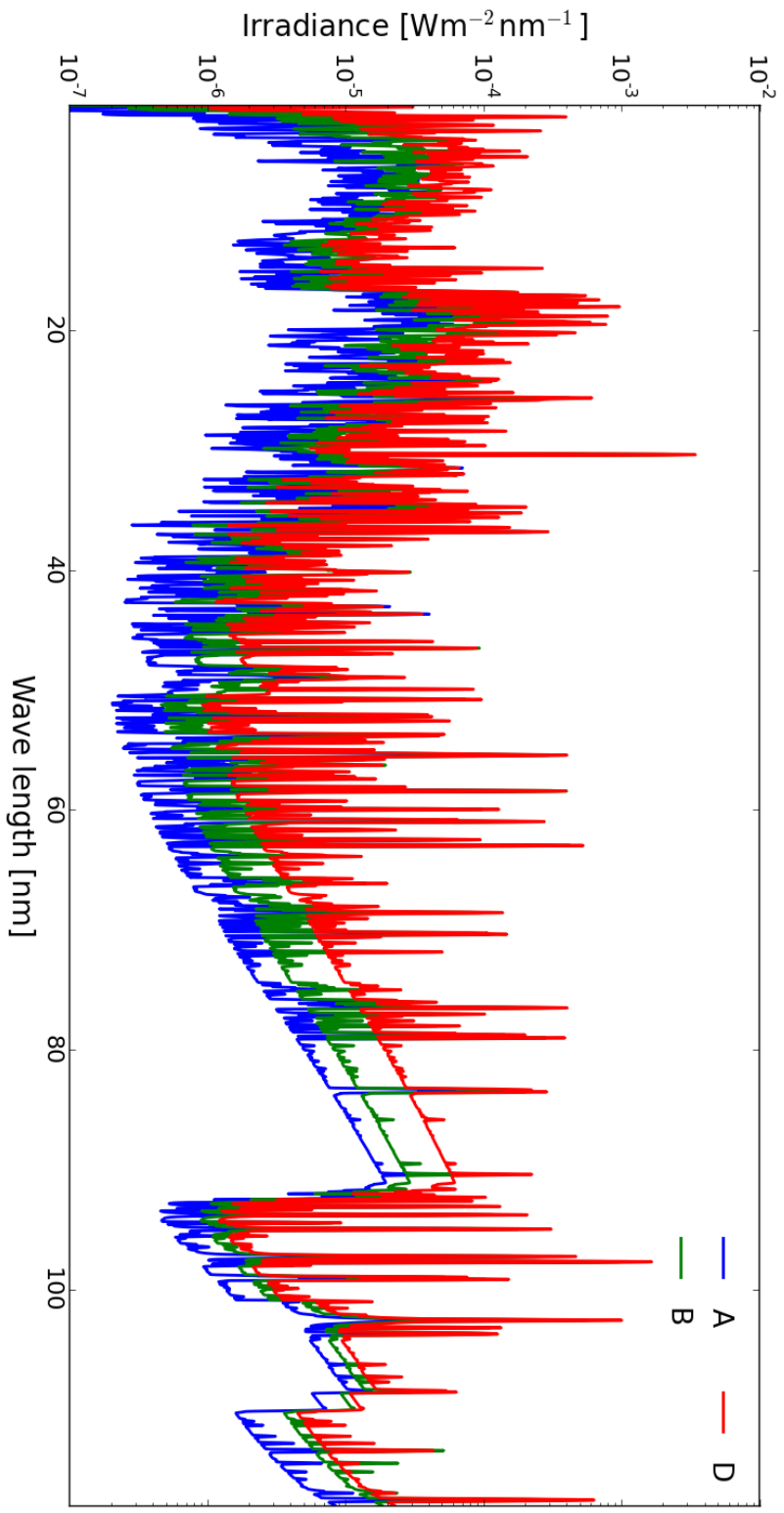

FIGURE 4.4: Components of the quiet Sun: dark-quiet-Sun inter-network (A), quiet-Sun inter-network (B), quiet-Sun network lane (D).

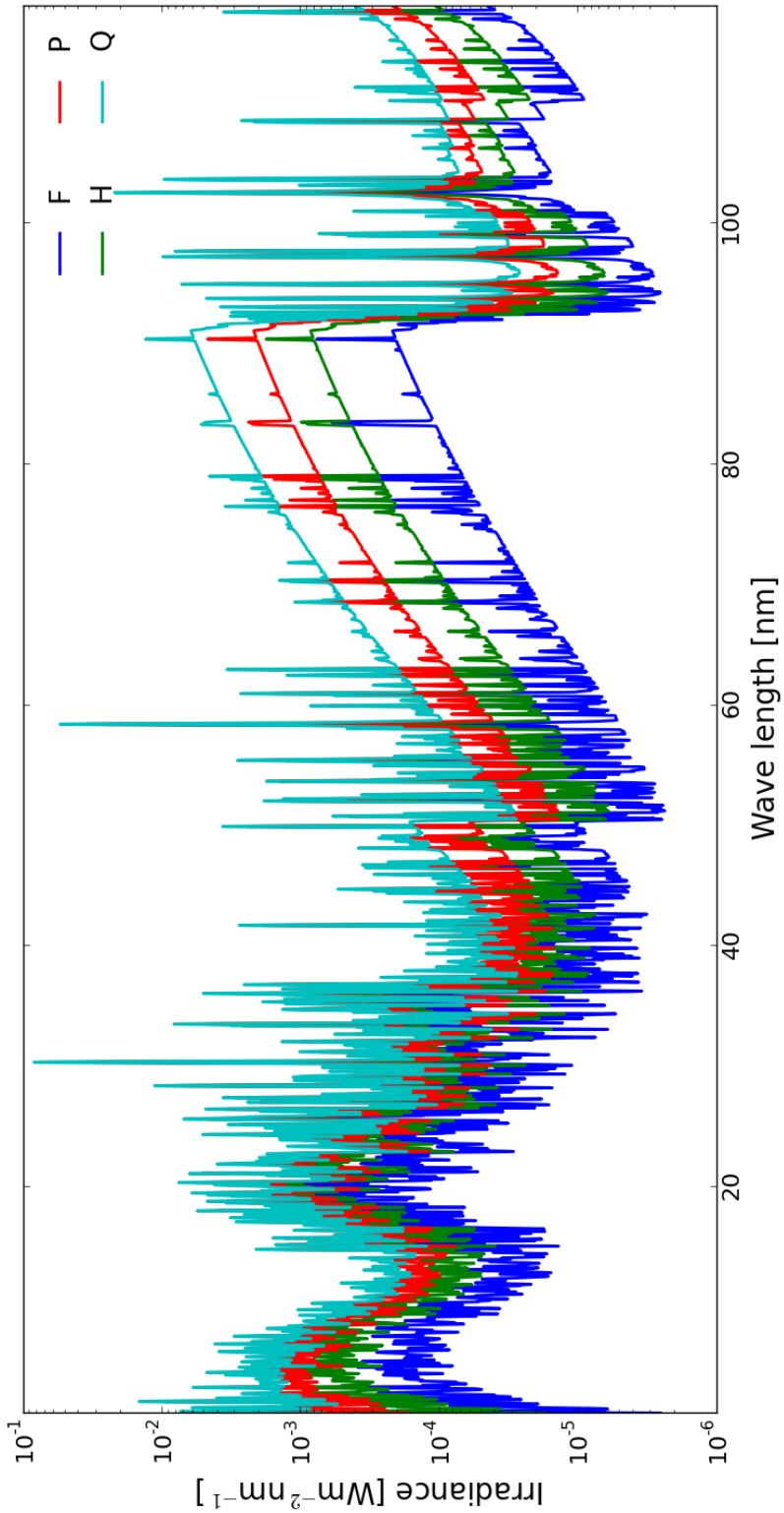

FIGURE 4.5: Components of the active Sun: enhanced network (F), plage (H), facula (P) and hot faculae (Q).

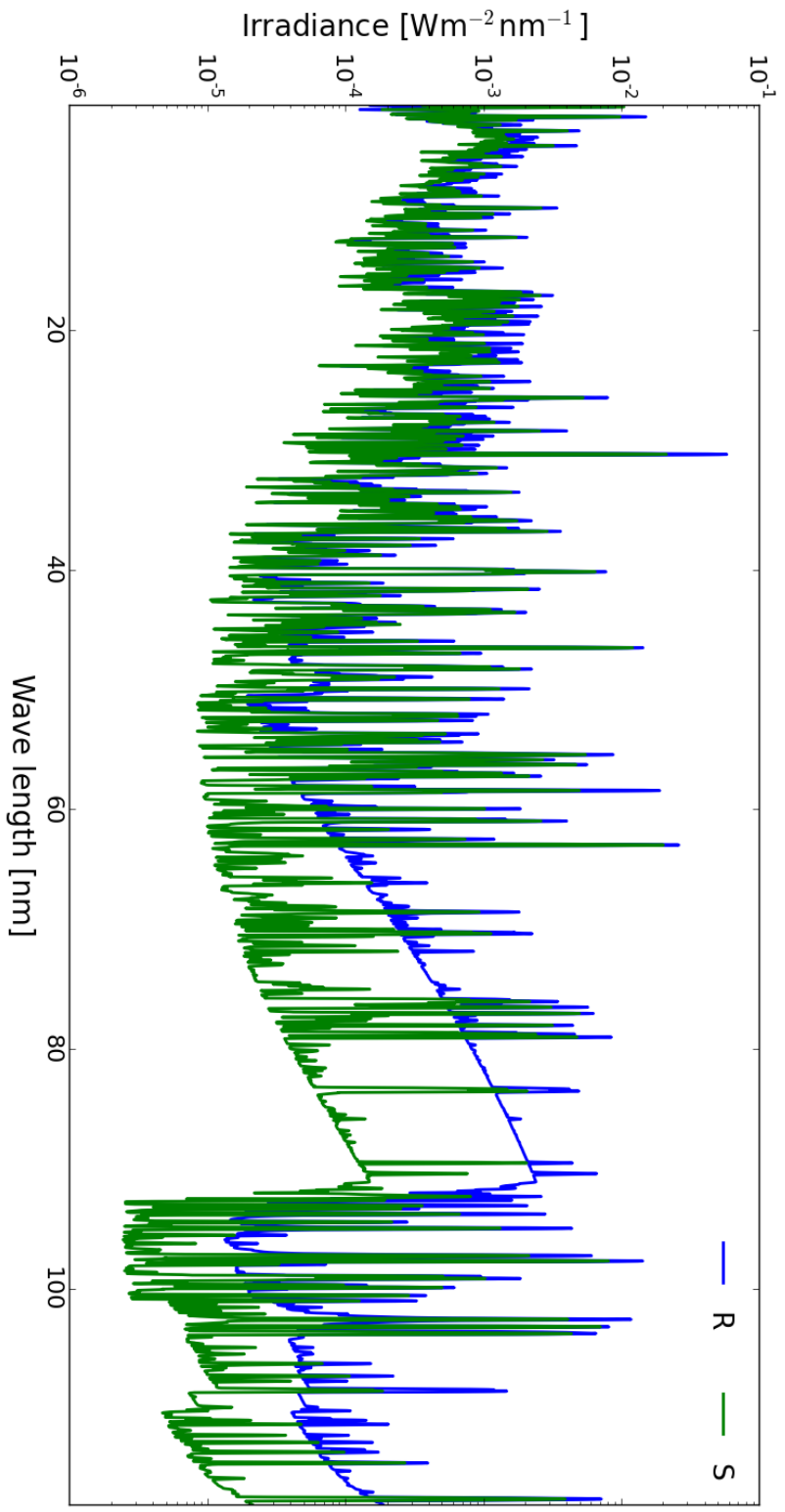

FIGURE 4.6: Components of the sunspots: sunspot umbra (S) and sunspot penumbra (R).

Chapter 5

Results

5.1 The sample

In Sec.2.2 we have discussed the modeling of stellar coronae and in Sec.4.4.2 we have presented the important relationships between plage and the other components. We now briefly present the sample stars used in this work.

The star with highest activity in our sample is EK Dra, a G 1.5 V star with an average rotation period of 2.68 days (Strassmeier and Rice, 1998;Messina and Guinan, 2003). Girardi et al. (2002) modeled EK Dra to have a radius of 0.95 $R_{\odot}$ with a mass of 1.06 solar masses. Montes et al. (2001a) and Montes et al. (2001b) concluded that EK Dra is a member of the Local Association or Pleiades group with an estimated age of 20-150 Myr. Wichmann, Schmitt, and Hubrig (2003) estimated an upper limit for EK Dra's age to be of 50-100 Myr. Here we adopt the same age as Ribas et al. (2005), namely 100 Myr. Baliunas et al. (1995) have shown that this star has no apparent chromospheric cycle if the S-index is considered.

Another young and well studied young solar analogue is π^1 UMa. With a spectral class of G1.5 V and a rotation period of about 4.9 days (Messina and Guinan, 2003). π^1 UMa is thought to be a member of the Ursa Major moving group (Montes et al., 2001a; Montes et al., 2001b; King et al., 2003) with an age of about 300 Myr years (e.g. Soderblom and Mayor, 1993). However, King et al. (2003), found a slightly older age of about 400-600 Myr. Here we adopt again the age used in Ribas et al. (2005) of 300 Myr. Girardi et al. (2002) found from evolutionary models that this star is only a few percent more massive and bigger than the Sun. Baliunas et al. (1995) have concluded that it shows no apparent cycle in the S-index and also it photometric variability is rather irregular.

β Com is a G05V star with a rotation period of about 12 days (Gray and Baliunas, 1997). Girardi et al. (2002) concluded from evolutionary models that this star is about 10 % more massive than the Sun with an age of about 2.3 ($\pm$ 1.1) Gyr. We again adopt the age from Ribas et al. (2005) with 1.6 Gyr. As this star is already more evolved than the previously mentioned solar proxies, it shows a rather regular pattern in the chromospheric activity already (Baliunas et al., 1995), with slighter smaller variations than the other young solar analogs.

Tab.5.1 shows all stars used in this study and their most important parameters.

Star	Spectral Type	Age [Gyr]	Rotation Period [d]	S-index
EK Dra	G1.5 V	0.1	2.68	0.554
π^1 UMa	G1.5 V	0.3	4.9	0.367
β Com	G0 V	1.6	12	0.201
Sun	G2 V	4.6	25.4	0.179

TABLE 5.1: Parameters for the stars used in this work. The S-index is the average given in Baliunas et al. (1995)

5.2 The solar model

For our comparison we adopt a solar model, which should represent the average solar XUV spectrum. Shapiro et al. (2014) give an average S-index for the Sun of 0.179 which results in the fraction of plage coverage A_H = 1.76 % and a spot coverage of 0.1%. We divide the spot coverage in contributions due to the umbra and penumbra and fill the star up with the other components according to the relationships given in Sec. 4.4.2. The result is shown in Fig.5.3. We take this solar spectrum to be an average spectrum based on the average S-index. The resulting spot coverage of 0.1% if compared with Fig.3.6 is an average for the last cycles.

5.3 The stellar models

In Tab. 5.2 we present the coverages by the different components according to our scaling laws based on the plage coverage, which in turn follows from the S-index:

Star	A+B	D	F	H	P+Q R	S	
EK Dra	0.	0.	0.	0.529	0.411	$8.57\cdot 10^{-3}$	$5.14\cdot 10^{-2}$
π^1 UMa	0.	0.	0.469	0.281	0.221	$4.29\cdot 10^{-3}$	$2.57\cdot 10^{-2}$
β Com	0.653	0.161	0.121	0.048	0.010	$9.04\cdot 10^{-4}$	$5.42\cdot 10^{-3}$
Sun	0.750	0.185	0.044	0.018	0.003	$1.40\cdot 10^{-4}$	$8.43\cdot 10^{-4}$

TABLE 5.2: Filling factors that were obtained with Eq.4.1 to 4.6in Sec.4.4.2

We see that EK Dra only contains the two facular components, as well as the two spot components and plage. We note that the scaling for the facular components according to Eq. 4.4 does not hold for EK Dra, as this would predict a coverage of hot faculae and faculae of about 75%. All together this would yield a coverage of 134% in total for EK Dra, which is physically not possible. We therefore only scale the spots according to the given relations for plage and spots and then fill the "rest" of the star then up with the facular components.
π^1 UMa on the other hand shows coverages with nearly all components, and the scaling for the facular components still holds. For this star already one of the lower-activity components, the enhanced network (component F) has to be taken into account that dominates over plage and faculae coverage. We see a trend that components with lower activity will start to dominate in coverage and irradiance (and flux therefore) for older stars.
We use β Com as an older solar analogue and we see that plage, faculae and spots no longer dominate and the enhanced network and the quiet Sun components A, B and D start to take over.
For the Sun, Fontenla et al. (2011) have shown that the most coverage on the Sun is

taken by the quiet Sun components and this is also the case in our assumed average solar spectrum.

Fontenla et al. (2009) have shown that up to a wavelength of 60 nm the corona dominates as without a coronal model the modeled spectra do not correspond to the observations. Unfortunately our spectral components also include the corona. This is problematic, as this is only a solar corona, which is cooler than the coronae of the younger, more active analogues and emits mostly in the soft X-ray, whereas the younger Suns emit more in harder X-rays. Fig.5.1 shows the spectrum for EK Dra obtained from the Fontenla models and the coronal model that was derived from X-ray spectra modeled with XSpec. It is clearly visible that our XUV spectrum is not able to reproduce EK Dra's corona, as our model corona is too cool and too soft. Therefore, the last step that needs to be done for all of our sample stars is to "fix" the X-rays. We take a compromise, when merging the XSpec and modeled spectrum together. A prominent line in the solar spectrum is HeI at 58.4 nm, formed at temperatures of about 32 000 K. This is below the temperature of the corona and thus below the assumed plasma temperature in the XSpec models. From HeI on, all lines are formed below 1 MK. We therefore expect that the coronal model does not hold for wavelengths below 58.4 nm and set our cut-off point for the XSpec spectra shortward of this line and then continue with the modeled spectra that were obtained by using the solar spectral features. Fig. 5.2 shows the modeled X-ray spectra for the sample stars. The difference between EK Dra and the older stars from the sample is clearly visible. EK Dra shows more emission in the hard X-rays, but towards the soft X-rays, π^1 UMa and β Com become stronger as well.

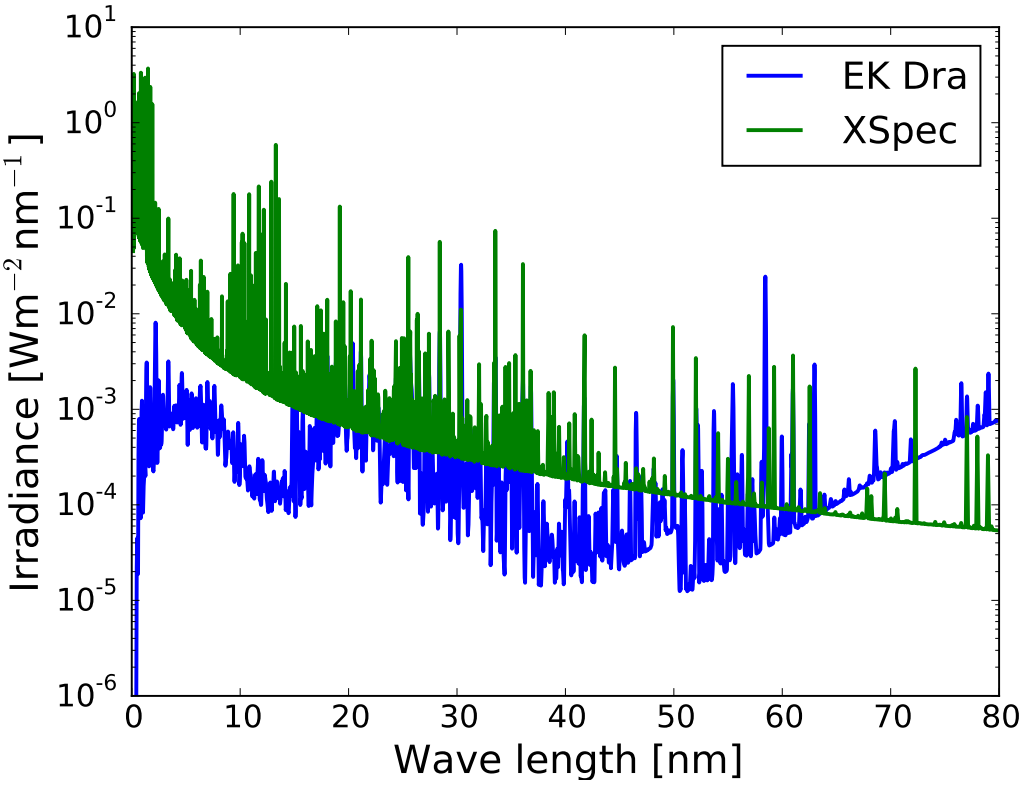

FIGURE 5.1: Comparison between the X-ray spectrum obtained with XSpec and the XUV spectrum. It is noticeable, that the current spectra do not fit the observed (and modeled) X-rays.

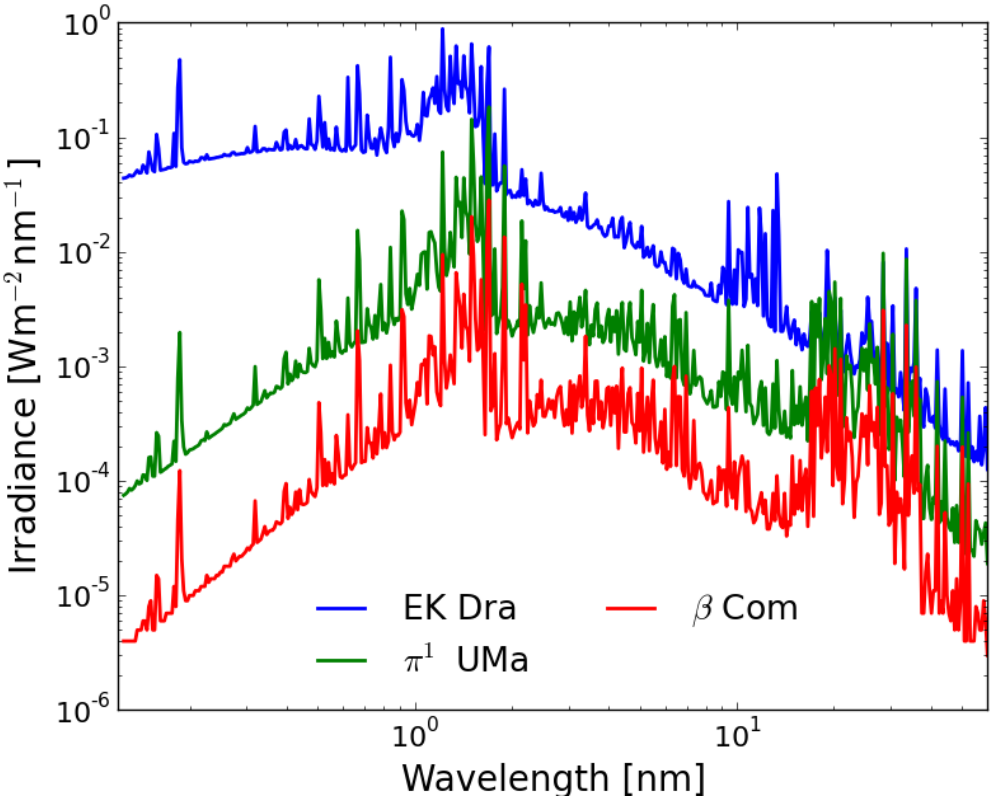

FIGURE 5.2: The modeled X-ray spectra of the sample stars.

Tab. 5.3 gives the integrated fluxes in different wavelength regimes for our sample stars. The younger stars in our sample, EK Dra and π^1 UMa, emit clearly stronger in the XUV than β Com and the Sun. With π^1 UMa being 200 Myr older than EK Dra, this would mean that hard X-ray emission already decreases by on order of magnitude during these early times, but the other fluxes have a less steep decline. Fig. 5.3 presents the set of spectra for the sample stars. The corona with the stars (except for the Sun) are similar in terms of lines and show a variation from the solar spectrum. This is because we did not compute a solar X-rays model, but used the corona that was included in the spectral features. The difference between the spectra is clearly visible. For the sake of getting a better impression of the shape of the spectra as well, all spectra have been binned to 1 nm. It seems that for the younger stars lines in the EUV are less intense with respect to the continuum compared to the solar spectra. We will discuss this in more detail on the examples of several lines in Sec. 5.4.3

Wavelength [nm]	EK Dra	π^1 UMa	β Com	Sun
0.12-2	$3.00\cdot 10^{-1}$	$2.50\cdot 10^{-2}$	$3.50\cdot 10^{-3}$	$1.36\cdot 10^{-5}$
2-10	$9.50\cdot 10^{-2}$	$1.42\cdot 10^{-2}$	$2.80\cdot 10^{-3}$	$3.39\cdot 10^{-4}$
10-36	$8.40\cdot 10^{-2}$	$3.10\cdot 10^{-2}$	$7.60\cdot 10^{-3}$	$2.05\cdot 10^{-3}$
36-92	$3.59\cdot 10^{-2}$	$1.97\cdot 10^{-2}$	$2.80\cdot 10^{-3}$	$2.44\cdot 10^{-3}$
92-118	$5.94\cdot 10^{-3}$	$3.95\cdot 10^{-3}$	$8.65\cdot 10^{-4}$	$5.97\cdot 10^{-4}$

TABLE 5.3: Integrated fluxes. Fluxes are in W m^{-2}

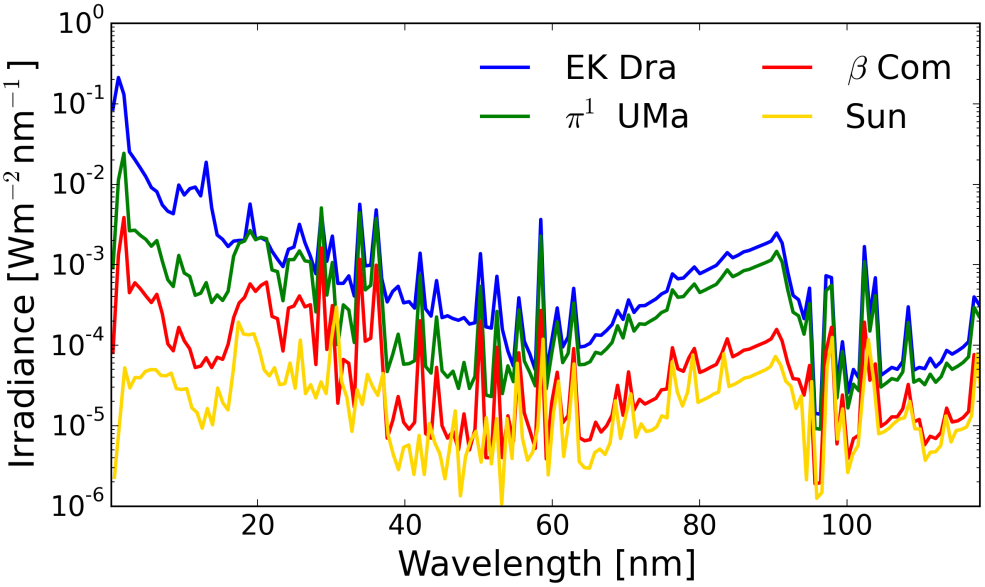

FIGURE 5.3: Spectra for the sample stars from 0.124 - 118 nm

Fig. 5.4 shows the fits for the different wavelength regimes in Tab. 5.3 and Tab. 5.4 gives the fitting parameters for the assumed power law in the form of

$$log(\text{flux}) = \alpha \cdot P_{rot}[d]^{\beta} \tag{5.1}$$

It is noticeable that the different regimes do not decay in the same way and that the power law indices become smaller towards the longer wavelengths. The evolution in the hard X-rays is the most drastic one, whereas the 92-118 nm regime shows the lowest power law index.

Wavelength [nm]	α	β
0.124-2	-0.34	0.82
2-10	-0.79	0.46
10-36	-0.8	0.38
36-92	-1.07	0.32
90-118	-1.86	0.18

TABLE 5.4: Fits to the data.

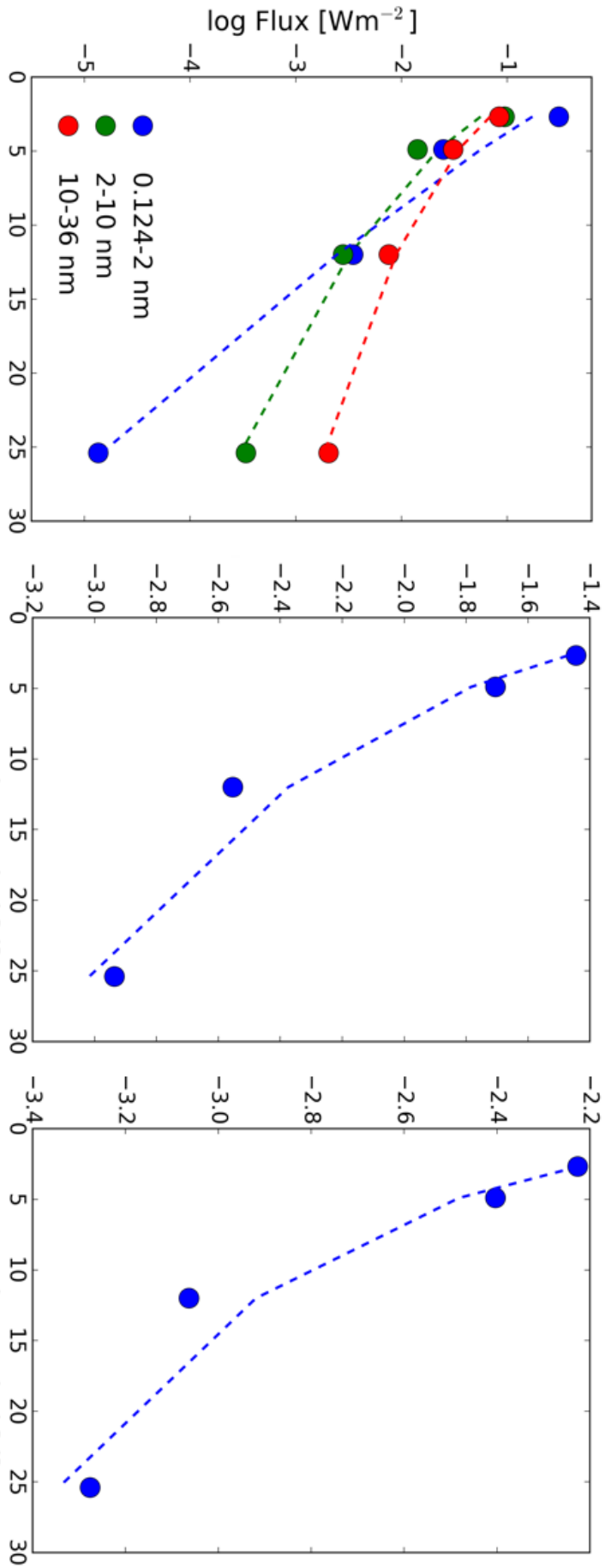

FIGURE 5.4: Fits to the different integrated fluxes in the regimes given by Tab. 5.3. Left: Fits to the X-ray regime, middle: the 36-92 nm regime, right: the 92-118 nm regime.

5.4 Comparison

5.4.1 36-92 nm

R05 obtained the fluxes by using an interpolation between the adjacent wavelength regimes. We test how good our values are compared to the R05 estimations (Table 5.5).

Star	Model	Model w/o c	R05
EK Dra	$3.59 \cdot 10^{-2}$	$3.05 \cdot 10^{-2}$	$4.56 \cdot 10^{-2}$
π^1 UMa	$1.97 \cdot 10^{-2}$	$1.83 \cdot 10^{-2}$	$1.52 \cdot 10^{-2}$
β Com	$2.80 \cdot 10^{-3}$	$2.35 \cdot 10^{-3}$	$2.85 \cdot 10^{-3}$

TABLE 5.5: Integrated fluxes for the spectral components. It is assumed that the area coverage for each of the components is 100 %. "Model w/o c" means the integrated fluxes of the modeled spectra without the fixed corona. Fluxes are in W m^{-2}

As can be seen, the models with the correct corona are in very good agreement with the R05 study. We have stated in the previous section that the solar spectral features include the solar corona that is too cool for our sample stars. Using the coronal models obtained with XSpec, we put the modeled spectra together at the 58.4 nm. This means that also the range 36-58.4 nm is affected by using the coronal models. In Tab. 5.5 we show both the fluxes with the "fixed" corona from the XSpec modeling and the "original" solar corona from the spectral features. These fluxes are on average 10 % smaller for the sample stars in comparison. This shows, that the corona does play a role down into these wavelength regimes, but it is not necessarily dominating. From Tab. 5.6 we see that for all of the sample stars it is possible to explain the reported fluxes with several components.

Component	36-92 nm	92-118 nm
A	$4.41 \cdot 10^{-4}$	$2.67 \cdot 10^{-4}$
B	$8.01 \cdot 10^{-4}$	$5.18 \cdot 10^{-4}$
D	$1.37 \cdot 10^{-3}$	$7.81 \cdot 10^{-4}$
F	$4.27 \cdot 10^{-3}$	$1.67 \cdot 10^{-3}$
H	$1.28 \cdot 10^{-2}$	$3.16 \cdot 10^{-3}$
P	$3.23 \cdot 10^{-2}$	$6.90 \cdot 10^{-3}$
Q	$7.69 \cdot 10^{-2}$	$1.24 \cdot 10^{-2}$
R	$4.63 \cdot 10^{-2}$	$1.00 \cdot 10^{-2}$
S	$1.63 \cdot 10^{-2}$	$4.18 \cdot 10^{-3}$

TABLE 5.6: Integrated fluxes for the spectral components. It is assumed that the area coverage for each of the components is 100 %. Fluxes are in W m^{-2}

5.4.2 92-118 nm

Tab.5.7 shows the integrated flux for our sample stars. We compare these fluxes in the same table with the results from R05. The values in parenthesis were obtained in R05 using an extrapolation to measurements from other stars in the sample. We see that the model and R05 fluxes for π^1 UMa are within a factor of 2. The same also holds for the solar fluxes as well. R05 used interpolations for the fluxes from three stars with ages of 0.3, 0.7 and 4.6 Gyr, to obtain fluxes for EK Dra and β Com. One problem with using the

Sun for such interpolations is that the Sun as well varies over the cycle and also from cycle to cycle variations are expected. Especially the case of cycle 19 in Foukal, 1998 raises some questions, as the spot coverage seems to be around the same as for cycles 16-18 and 20, but the plage coverage is higher. This indicates that this cycle might have been more enhanced in plage coverage, which would likely result in a higher contribution of the plage to the flux in the short wavelength regime. R05 used measurements from 1993. In that time the Sun was in mid cycle 22, which also might represent an average value for the Sun. However, with the variations in cycle strengths from cycle to cycle, there might be a variation of flux depending on which cycle is considered. We will discuss this later in Sec. 5.7.

Star	Model	R05	Ratio
EK Dra	$5.94 \cdot 10^{-3}$	$(1.81 \cdot 10^{-2})$	3.1
π^1 UMa	$3.948 \cdot 10^{-3}$	$8.38 \cdot 10^{-3}$	2.1
β Com	$8.16 \cdot 10^{-4}$	$(1.70 \cdot 10^{-3})$	2.1
Sun	$1.50 \cdot 10^{-3}$	$7.40 \cdot 10^{-4}$	0.5

TABLE 5.7: Comparison between our modeled fluxes (Model) and the reported values in Ribas et al. (2005). "Ratio" denotes the ratio between the reported and modeled values. Fluxes are in W m^{-2}

The fluxes in the 92-118 nm range are lower in our models for all young solar analogs than the values given in R05. EK Dra has the problem that with our modeling, we can only scale plage and the two spot components, as Eq. 4.4 would already predict a higher coverage of the facular components than physically possible. If we take the reported fluxes in R05 for granted, it is interesting to look, if we are actually able to match this flux with any our spectral components. Going back to Tab. 5.6 we see that none of the components can match the reported flux of $1.81 \cdot 10^{-2}$ W m^{-2} for EK Dra even if one of them would fill 100 % of the surface. The highest possible value is achieved by the hot faculae (component Q) with $1.24 \cdot 10^{-2}$ W m^{-2}. For the other stars in the sample, several components and their combinations are able to match the observed fluxes. We will discuss later the effects of different input parameters for plage and spot coverage in the cases of π^1 UMa and β Com, but first we want to discuss fluxes of some selected lines.

5.4.3 Line fluxes

In Tab. 5.8, 5.9 and 5.10 we compare the line fluxes for CIII at 97.7 nm, the OI triplet centered at 130.4 nm and CIV at 155 nm, respectively between our models and observations. It is striking that our model is not able to explain the observed values for EK Dra. Especially for the youngest solar analogs the obtained fluxes show a significant difference between the model and the observations. Why we are actually not able to reproduce the observed fluxes is shown in Table 5.11

Star	Flux	R05	Ratio
EK Dra	$5.00\cdot 10^{-4}$	$5.00\cdot 10^{-3}$	10
π^1 UMa	$4.03\cdot 10^{-4}$	$1.20\cdot 10^{-3}$	3
β Com	$1.22\cdot 10^{-4}$	$3.00\cdot 10^{-4}$	2
Sun	$8.65\cdot 10^{-5}$	$1.50\cdot 10^{-4}$	2

TABLE 5.8: Comparison of the modeled fluxes of CIII at 97.7 nm. R05 denotes the values given in Ribas et al. (2005). "Ratio" gives the ratio between the reported flux and our modeled fluxes. Fluxes are in W m^{-2}

Star	Flux	R05	Ratio
EK Dra	$4.29\cdot 10^{-4}$	$4.30\cdot 10^{-3}$	10
π^1UMa	$3.31\cdot 10^{-4}$	$1.18\cdot 10^{-3}$	4
βCom	$1.26\cdot 10^{-4}$	$4.50\cdot 10^{-4}$	4
Sun	$1.07\cdot 10^{-4}$	$1.43\cdot 10^{-4}$	1

TABLE 5.9: Same as Table 5.8 but for the OI triplett centered at 130.4 nm.

Star	Flux	R05	Ratio
EK Dra	$3.80\cdot 10^{-4}$	$9.00\cdot 10^{-3}$	24
π^1 UMa	$2.81\cdot 10^{-4}$	$2.21\cdot 10^{-3}$	8
β Com	$4.46\cdot 10^{-5}$	$4.00\cdot 10^{-4}$	7
Sun	$3.26\cdot 10^{-5}$	$1.47\cdot 10^{-4}$	5

TABLE 5.10: Same as Table 5.8 but for CIV at 155 nm

Component	OI	CIII	CIV
A	$7.11\cdot 10^{-5}$	$3.652\cdot 10^{-5}$	$5.26\cdot 10^{-5}$
B	$1.20\cdot 10^{-4}$	$1.010\cdot 10^{-4}$	$8.30\cdot 10^{-5}$
D	$1.05\cdot 10^{-4}$	$1.700\cdot 10^{-4}$	$1.03\cdot 10^{-4}$
F	$2.24\cdot 10^{-4}$	$2.920\cdot 10^{-4}$	$1.69\cdot 10^{-4}$
H	$3.17\cdot 10^{-4}$	$2.940\cdot 10^{-4}$	$2.47\cdot 10^{-4}$
P	$5.31\cdot 10^{-4}$	$6.140\cdot 10^{-4}$	$4.63\cdot 10^{-4}$
Q	$7.46\cdot 10^{-4}$	$8.100\cdot 10^{-4}$	$6.13\cdot 10^{-4}$
R	$3.71\cdot 10^{-4}$	$1.400\cdot 10^{-3}$	$8.26\cdot 10^{-4}$
S	$8.09\cdot 10^{-6}$	$7.900\cdot 10^{-4}$	$4.11\cdot 10^{-4}$

TABLE 5.11: Comparison of the lines fluxes of OI, CIII and CIV; the values are given as if the star was fully covered by this one particular component each.Fluxes are in W m^{-2}.

For EK Dra, none of the components is able to explain the observed fluxes. For π^1 UMa, only component R is in the same order of magnitude for CIII; for the other lines, no component can match the observations. In contrast, β Comae's line fluxes could be reached with several components for all lines. However, we note that the reported fluxes in R05 in this wavelength regime have errors between 10-40 %. Considering a maximum error of 40%, our fluxes are in better agreement, but still may represent a lower limit. This of course is a limitation that comes with using solar spectral features. But why are we able to match the reported integrated fluxes in the range 36- 92 nm range, do well in the 92-118 nm regime (except for EK Dra), but cannot match the reported line fluxes?

This issue can be already seen in the spectra of the components each (Fig.4.4, 4.5 and 4.6). The difference between the spectral components is overall more pronounced in the continuum and the shape of the spectra, than in the spectral lines itself. CIII and CIV are lines that are mostly formed in the transition region. It is possible, that this specific layer of the atmosphere, in which the stars are formed, is more dense compared to the Sun.

The spectra presented in the previous section were obtained using the average S-index for our sample stars given in Baliunas et al. (1995). We focus mostly on the parts between 36-92 nm. As the X-ray spectra have been modeled using XSpec, the rest of the spectrum can be modified using different coverage for the components. We will especially focus in plage and spots.

5.5 Effect of plage coverage

5.5.1 π^1 UMa

From Baliunas et al. (1995) we find that the highest S-index was 0.4 whereas the lowest was 0.338. Using Eq.4.1 and Eq.4.2 we get a plage coverage of 32.7 and 24.2 % and a spot coverage of 3.3 % and 2.2%, respectively. Using all other scaling relations again, we get total integrated flux from 36-92 nm of $2.36 \cdot 10^{-2}$ and $1.66 \cdot 10^{-2}$ W m^{-2} for the high and low case, respectively. The ratio between those two cases is 1.4. For 92-118 nm we obtain $4.62 \cdot 10^{-3}$ and $3.41 \cdot 10^{-3}$ W m^{-2} for the higher and lower activity case. This corresponds to a factor of 1.3 difference. Tab. 5.12 gives the filling factors and Tab. 5.13 gives the integrated fluxes for each case. Comparing the two mentioned wavelength regimes, it is evident that the variability of the S-index has the same effect on both regimes. In Fig. 5.5 the three spectra are shown. We only show the spectrum starting at $\approx$ 50 nm, as below the corona dominates and the corona is the same for all three examples.

Case	F	H	P+Q	R	S
High	0.35	0.33	0.29	$4.57 \cdot 10^{-3}$	$2.74 \cdot 10^{-2}$
Average	0.47	0.28	0.22	$4.29 \cdot 10^{-3}$	$2.57 \cdot 10^{-2}$
Low	0.57	0.24	0.16	$3.14 \cdot 10^{-3}$	$1.89 \cdot 10^{-2}$

TABLE 5.12: Filling factors for testing different S-indices for π^1 UMa. High, average and low refer to an S-index of 0.4, 0.367 and 3.41, respectively. Components A+B and D are not included as their contribution is 0%

Case	36-92	92-118
High	$2.36 \cdot 10^{-2}$	$4.62 \cdot 10^{-3}$
Average	$2.00 \cdot 10^{-2}$	$3.95 \cdot 10^{-3}$
Low	$1.66 \cdot 10^{-2}$	$3.41 \cdot 10^{-3}$

TABLE 5.13: Integrated fluxes for two different regimes for the filling factors given in Tab. 5.12. Fluxes are in W m^{-2}

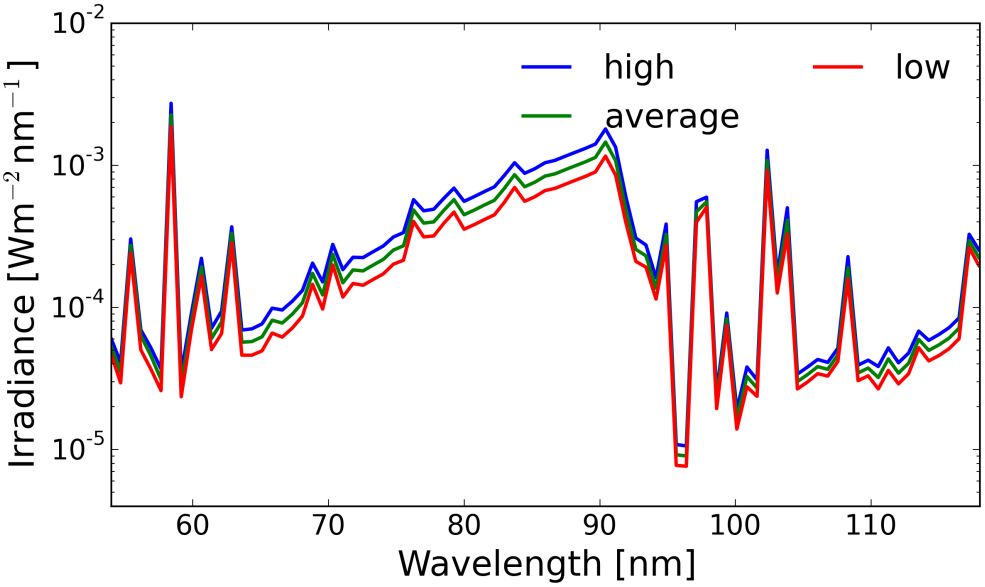

FIGURE 5.5: Spectrum of π^1UMa with the filling factors given in Tab. 5.12. This shows the difference of the chosen S-index.

5.5.2 β Com

We now discuss β Com. This star is older than π^1UMa, has a lower S-index and is less active than the younger star. We again first only vary the S-index: 0.228, 0.201 and 0.182 for a high, average and low activity level in this order. Tab. 5.14 and Tab. 5.15 present the coverages for each component and the integrated fluxes. The resulting fluxes between 36-92 nm are a factor of 3 different between high and low and for the regime 92-118 nm the difference is even a bit smaller with a factor of 2. This means that β Com shows a larger variation in the cycle if the S-index is considered compared to π^1UMa. Still, we note that the measurements for π^1UMa of the MWO sample are might not be long enough to reveal the full variation of this young Sun.

Case	A+B	D	F	H	P+Q	R	S
High	0.53	0.13	0.22	0.09	$2.56\cdot 10^{-2}$	$2.62\cdot 10^{-3}$	$1.57\cdot 10^{-2}$
Average	0.65	0.16	0.12	0.05	$9.93\cdot 10^{-3}$	$9.04\cdot 10^{-4}$	$5.42\cdot 10^{-3}$
Low	0.74	0.18	0.05	0.02	$3.23\cdot 10^{-3}$	$2.11\cdot 10^{-4}$	$1.27\cdot 10^{-3}$

TABLE 5.14: Filling factors for testing different S-indices for β Com. High, average and low refer to an S-index of 0.228, 0.201 and 0.182, respectively.

Case	36-92	92-118
High	$4.30\cdot 10^{-3}$	$1.28\cdot 10^{-3}$
Average	$2.44\cdot 10^{-3}\cdot 10^{-3}$	$8.64\cdot 10^{-4}$
Low	$1.43\cdot 10^{-3}$	$6.29\cdot 10^{-4}$

TABLE 5.15: Integrated fluxes for two different regimes for the filling factors given in Tab. 5.14. Fluxes are in W m^{-2}

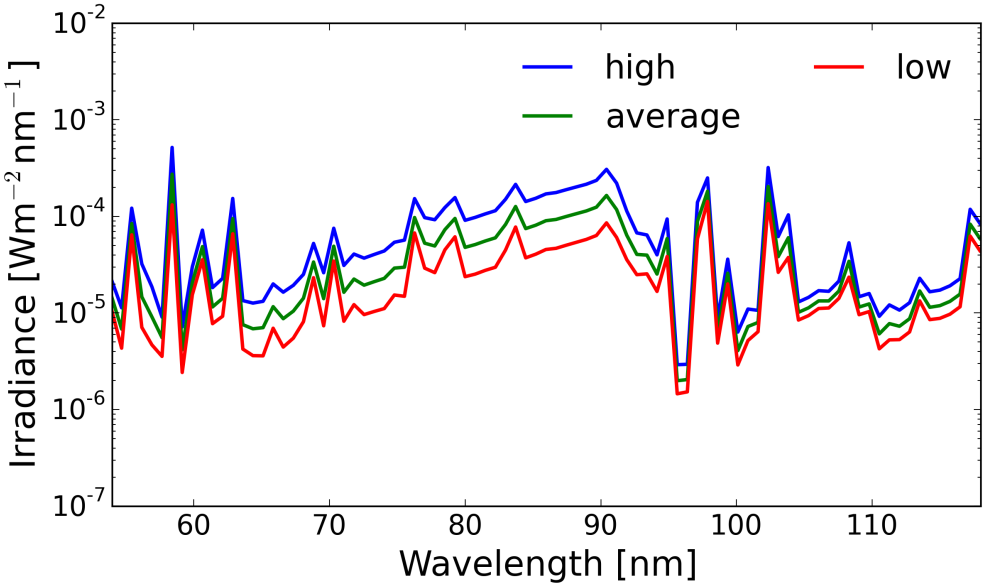

FIGURE 5.6: Spectrum of β Com with the filling factors given in Tab. 5.14. This shows the difference of the chosen S-index.

5.6 Effect of spot coverage in the case of π^1 UMa

We have seen that a different plage coverage can make already a difference, but what about the contribution from spots? We discussed that obtaining spot coverages has its difficulties and for the sake of consistency we used spot coverages for EK Dra that were obtained from light curve modeling and calculated from the difference in photometric variability spot coverages for other stars. Let us now assume that we do not distinguish between the way the spot coverages were obtained and assume that EK Dra has either 11% Strassmeier and Rice (1998) or 44% O'Neal et al. (2004) spot coverage. With the difference in photometric variability between EK Dra and π^1UMa, this results in 5% and 18% spot coverage for the latter. We now assume that π^1 UMa is at its maximum of the S-index, therefore has a corresponding plage coverage of 32.7 %. As the plage coverage is now kept constant and Eq.4.4 shows that the faculae correlates with the plage coverage, these two components do not vary. We have presented a equation in a previous section that gives a relation between the plage and spot coverage. In this study we now do not consider this equation anymore and assume that the new spot coverages are "measured" together with the plage indices given. The results for this study are shown in Table 5.16 (coverages) and Table5.17 (fluxes) and the spectra can be seen in Fig. 5.7. We find that the highest possible flux with 2.52$\cdot$ 10^{-2} between 36 and 92 nm and 5.18 $\cdot$ 10^{-3} W m^{-2} from 92-118 nm can be obtained using a spot coverage of 20% and a plage coverage of 32.7%. Comparing this to the results that were obtained in Sec.5 the flux with an assumed high spot coverage and a high S-index is 7% higher in the range 36-92 nm and 11 % higher in the range 92-118. Compared with the results that were obtained with the varying plage coverage, the difference induced by spot coverage variations is less pronounced, but the resulting fluxes are higher than in the previous cases.

Spot coverage	F	H	P+Q	R	S
3%	0.35	0.33	0.29	$4.29 \cdot 10^{-3}$	$2.57 \cdot 10^{-2}$
5%	0.33	0.33	0.29	$7.14 \cdot 10^{-3}$	$4.29 \cdot 10^{-2}$
20%	0.18	0.33	0.29	$2.86 \cdot 10^{-2}$	1.71e-01

TABLE 5.16: Test for different spot coverages for π^1 UMa. The plage coverage is calculated from the highest S-index for this star. Components A+B and D are not included as their contribution is 0%.

Spot coverage	36-92	92-118
3%	$2.36 \cdot 10^{-2}$	$4.61 \cdot 10^{-3}$
5%	$2.38 \cdot 10^{-2}$	$4.68 \cdot 10^{-3}$
18%	$2.52 \cdot 10^{-2}$	$5.11 \cdot 10^{-3}$

TABLE 5.17: Integrated fluxes in the EUVI and EUVII regime for the coverages given in Table5.16. Fluxes are in W m^{-2}

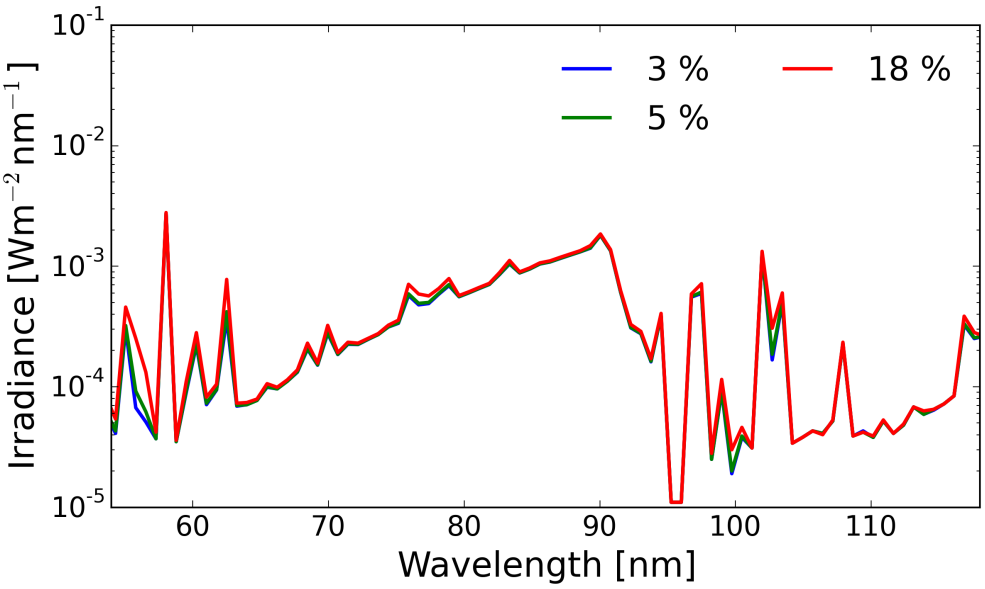

FIGURE 5.7: Spectrum of π^1 UMa with the filling factors given in Tab. 5.16. This shows the difference of the spectra with a high value of the S-index and different spot coverages given by the labels.

As we unfortunately do not have any photometric variability for β Com available, we refrain from performing another study that involves a varying spot coverage at this point. As in the case of π UMa, we will likely obtain higher fluxes with a higher spot coverage. We conclude that the choice in plage and spot coverage does make a difference in the spectra, even though the effect is not too severe.

We have discussed possible differences in the choice of the input parameters for our sample stars and find that with a higher plage and spot coverage for π^1UMa and a higher plage coverage for β Com the difference between the R05 values and the values in this work becomes smaller. In fact, for both star we are well within a factor of 2 of R05. Moreover the measurements for the sample star in R05 hold some errors as well.

For the *FUSE* measurements of πUMa, R05 states an error of about 10%-40% and claims that data are free of major flares. Still, microflares or smaller turbulences could affect the measurements and unfortunately R05 only use one measurement for the flux estimation in the case of π^1 UMa.

5.7 Solar cycle variations

Studying the evolution of the Sun in Time requires at some point to use a solar spectrum for comparison. R05 used a measurement from mid-cycle in cycle 22, whereas here we used the average S-index and plage and spot coverage from cycle 19. This particular cycle has been the most active cycle in the records. We use the coverage for the components presented in Fontenla et al. (2011) and use the cases labeled "peak" and "low". These represent cycle maximum and minimum of cycle 23. Fig. 5.8 and 5.9 show the two examples. In the range between 36-92 nm the offset between the two cases is roughly a factor of 2.5, in the range 92-118 nm, however, the ratio is already smaller with an offset of about 1.8. This shows once again that caution has to be taken in choosing the solar spectra for these kind of comparison, in addition to the stellar activity that has to taken into account as well. R05 especially showed the evolution of their sample stars with the respective fluxes to the Sun. A comparison like this only makes sense, if all stars are in the same cyclic state, while comparing stars in different cycle phases introduces deviation and scatter.

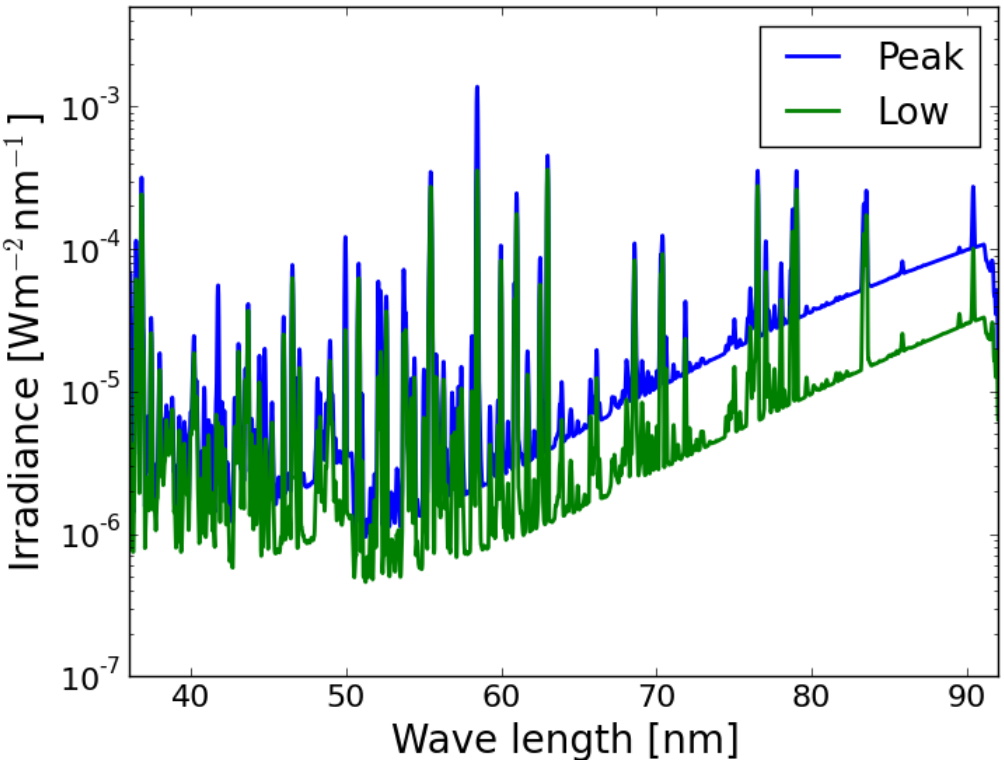

FIGURE 5.8: Comparison between two different cases from Fontenla et al. (2011) for the range 36-92 nm

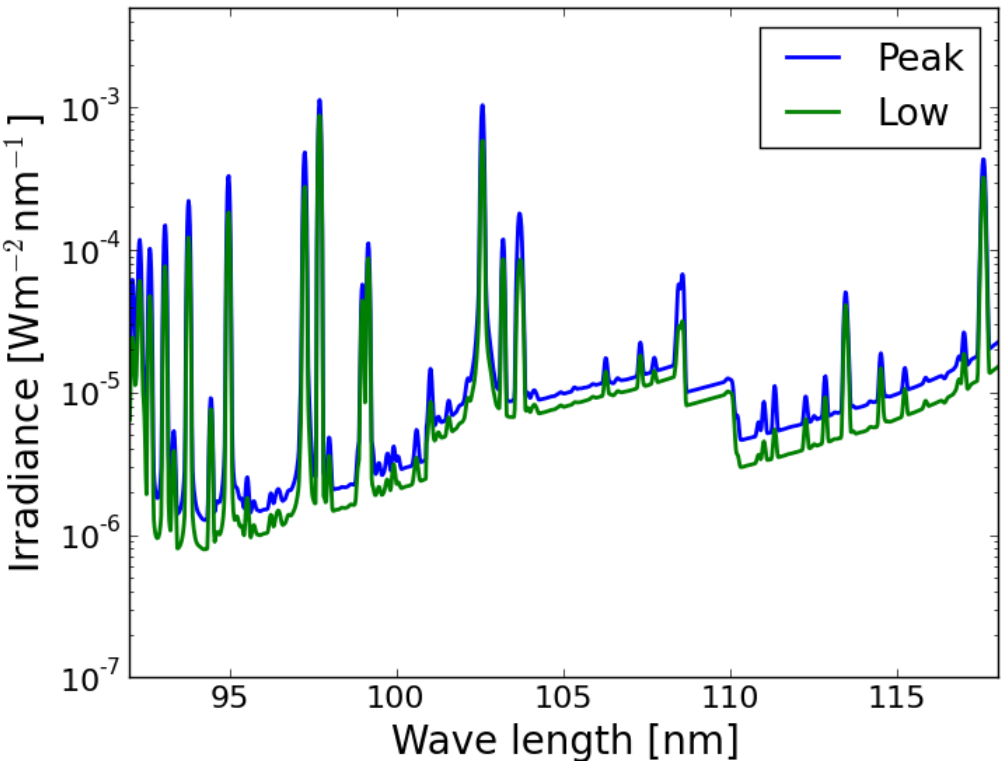

FIGURE 5.9: Comparison between two different cases from Fontenla et al. (2011) for the range 92-118 nm

5.8 Other effects and limitations

Another effect that has not been considered so far is the effect of a different inclination. Depending on how the star is inclined with respect to our line of sight, we might mostly see the polar regions, the equatorial region or a region in between. For the stars in this sample, we have not included the inclination. This of course could induce some errors, especially in the visible coverages and resulting fluxes. However, we are confident that we have a non-polar view on all of our sample stars.

We have seen that our solar spectral features are eventually not strong enough to precisely reproduce the observed fluxes if compared to previous studies. As we did not calculate the spectral components ourselves, we can only make assumptions on why this does not work. We have seen in the beginning that the coronae of younger, more active solar like stars are hotter than the solar corona. It is highly uncertain if that also means that the chromosphere is also hotter than the solar one, but we could assume that the density of the plasma in the more active stars might be higher, which would result eventually in higher fluxes. This study has been unique in the way of modeling and is the only one known to be able to also consider cyclic variability.

We may have a good estimate of plage coverage and a feeling for the spot coverages of the sample stars, but lack knowledge of the facular contribution on stars other than the Sun. The "normal" facula (P) and hot facula (Q) are strong components regarding their flux, so an underestimation of those two components may lead to lower fluxes than anticipated. On the Sun, it seems that there is some saturation value for both plage and faculae (Foukal, 1998). However, this "saturation" might be different on other stars.

As we were provided with solar spectra features that contain the solar corona, we had to model the coronal part up to approximately 60 nm, which gives rise to other uncertainties. Another effect that comes with using pre-calculated solar spectral features is the applicability to different spectral classes. We have shown that for G-type stars the models are consistent with measurements and previous studies, but problems may arise when using solar spectral features to non-G-type stars. In the bigger picture of evaluating habitability and atmospheric evaporation of planets, M dwarfs have been a topic of interest. These stars, however, give rise to other problems (different spectral class, temperature, metallicity) and unknowns (cycles, chromospheric activity from long term monitoring, etc.).
Lastly, we were able to consider effects of varying plage and spot coverage accounting for variability during a stellar activity cycle. We do not know in which cyclic state the stars and their reported fluxes in Ribas et al. (2005) were, as far as they have any cyclic behaviour, or in what state of any irregular variability. This will be important to consider in future studies.

Chapter 6

Concluding remarks and outlook

6.1 Summary

We have shown that it is possible to model stellar radiation for young solar analogs in the wavelength regime from 0.1 to 118 nm using a coronal model calculated with XSpec below $\approx$ 60 nm and a chromospheric model that is based on the S-index and plage coverage. The main findings are:

- The strongest decay in time is seen in the X-rays in between 0.124-2 nm with a power law index with 0.82.
- The decay between 36-92 and 92-118 nm follow a power law of index with 0.46 and 0.38, respectively.
- Using π^1 UMa and β Com we have shown that a variation in the S-index (and the resulting plage coverage) has an impact on the emitted flux, hence caution has to be taken when comparing measurements and models.
- This has also been shown in the case of π^1UMa, where we varied the spot coverage separately, even though the effect is smaller than the effect of the plage coverage.
- The cyclic variation also holds for the Sun, so one has to be careful in comparing stellar and solar fluxes.

The XUV evolution of solar-type stars, especially in the range 36-92 nm, might be more severe than previously expected. The influence of the corona has to be taken into account, as the models without the right coronal model have about 10% less integrated flux. The unique approach used in this work has shown that the stellar cyclic variability or generally speaking, the stellar variability in terms of coronal, chromospheric and photospheric activity has to be taken into account for modeling stellar XUV. Especially connecting solar variability and the understanding of the interplay between different activity parameters is a crucial aspect for this kind of studies.

6.2 Outlook - Planetary atmospheres

We have mentioned in the introduction that rocky planets form with an initial hydrogen envelope. The early Earth's atmosphere has been stripped off by the solar wind and the high energy radiation and the secondary atmosphere that was out-gased is still influenced heavily by our host star. Today's atmosphere of the Earth consists by volume predominantly of nitrogen and oxygen, with smaller amounts of argon and carbon dioxide. Also water vapor is present in various amounts. We have seen that the star's spectral behaviour changes with time, but the influence of the radiation on the atmosphere is not only given by the spectral irradiance, but also by the cross section of atoms

and molecules. Fig. 6.1 shows the cross section of the two most prominent molecules in the Earth's atmosphere. "Total" refers to the sum of the cross sections of all possible outcomes of the interaction with N_2 and O_2 and a photon of a certain wavelength (Huebner and Carpenter, 1979; Huebner and Carpenter, 1979; Huebner and Mukherjee, 2015). It is important to note that the cross section is not constant and varies over the wavelength regime shown over orders of magnitudes.

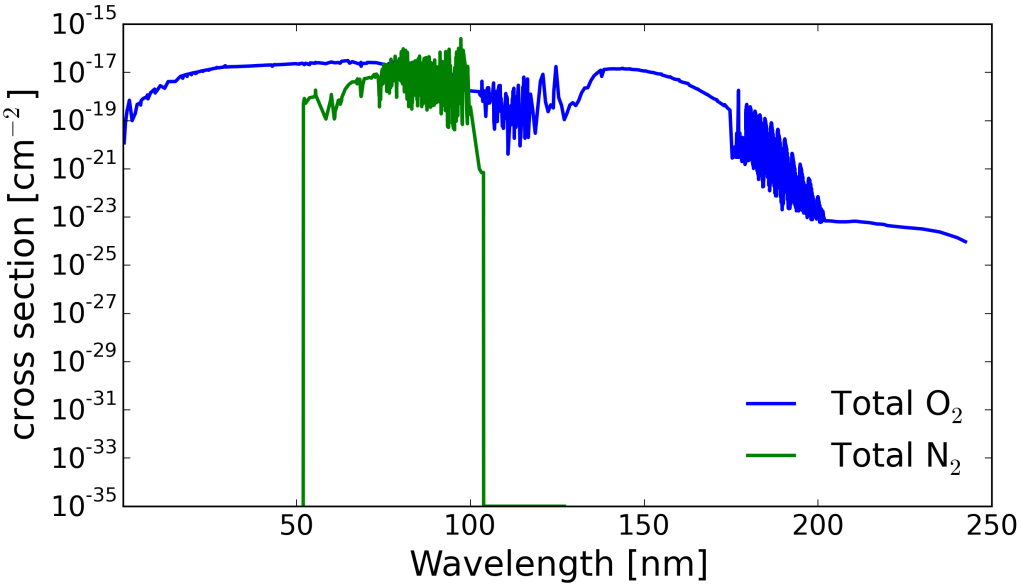

FIGURE 6.1: Cross section of O_2 and N_2 for all possible outcomes.

We shortly want to consider the reaction outcomes of O_2 and a photon in more detail, as this molecule has some important absorption features. Fig. 6.2 shows possible outcomes of the interaction between O_2 and a photon. D and S denote different excited states of oxygen and P denotes the ground state. This figure shows that the outcome of the reaction depends on the wavelength, so the energy of a photon. The outcome of $O^1(S) + O^1(S)$, for instance, is only likely with photons of the narrow wavelength regime from about 91-95 nm. On the other hand, in order to produce $O^3(P) + O^3(P)$ and $O^3(P) + O^1(D)$, two different wavelength regimes are favoured. Several bands can be seen in both spectra. Between about 67 and 100 nm lie the Hopfield bands and between 176 and 192.6 nm are the so-called Runge-Schumann bands. Moreover between 135 to 176 lies the Runge-Schumann continuum that shows rather strong absorption as well.

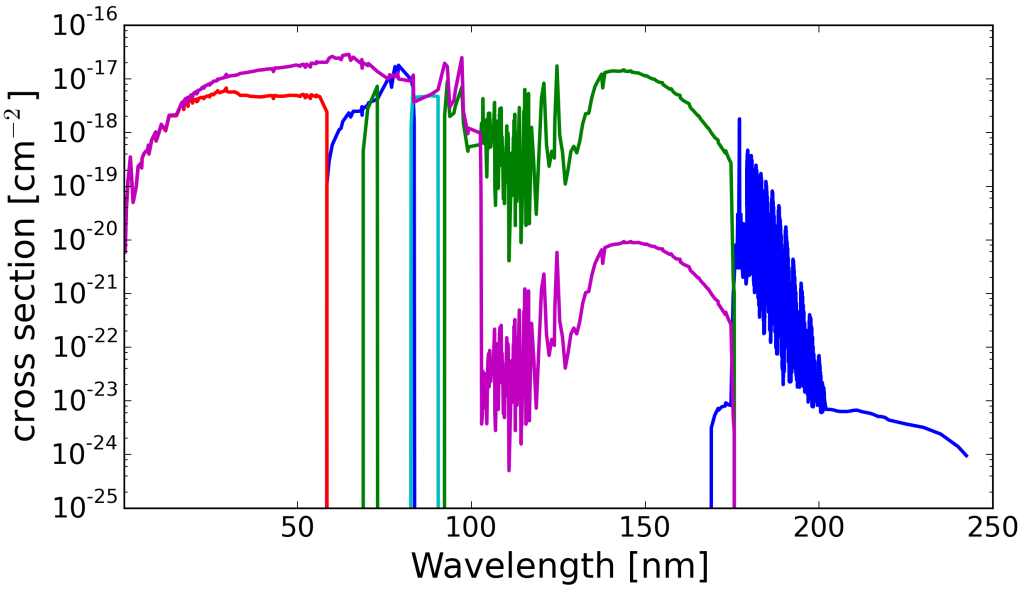

FIGURE 6.2: Cross section of various outcomes of the interaction with O_2 and a photon of a certain energy; Dark blue: $O(^3P)+O(^3P)$, green: $O(^3P)+O(^1D)$, red: O^++O+e, light blue: $O(^1S)+O(^1S)$, pink: 0_2^+ +e

Future studies will include hydrodynamic atmosphere models with several species and reaction rates in order to understand the evolution of the atmosphere of our own planet, moons in the solar system and exoplanets under the influence of the XUV radiation from the host star.

Zusammenfassung

Die Evolution der Röngten- und extrem ultravioletter Strahlung (XUV) ist wichtig um die Veränderungen von Planetenatmosphären zu verstehen. Die XUV-Strahlung von sonnenähnlichen Sternen variiert mit der Zeit, eine Abschwächung ist sichtbar in allen Wellenlängenbereichen. Wir präsentieren eine neue Methode um den Fluss im Bereich 36-92 nm zu modellieren. Aufgrund von interstellar Extinktion ist es nicht möglich in diesem Bereich Flüsse für Sterne, außer unserer Sonne, zu messen. Wir verwenden Sonnenspektralkomponenten, die anhand ihrer Füllfaktoren, die vom S-index berechnet worden sind, zusammenaddiert werden. Wir stellen fest, dass unsere Modelle konsistent sind mit der vorhandenen Literatur und sind fähig den Effekt der Variation im S-index auf die XUV Spektren unserer Beispielsterne zu untersuchen.

Bibliography

Ayres, T. R. et al. (1995). „The RIASS coronathon: Joint X-ray and ultraviolet observations of normal F-K stars“. In: *Astrophys. J. Suppl.* 96, pp. 223–259. DOI: 10.1086/192118.

Babcock, H. D. (1959). „The Sun's Polar Magnetic Field.“ In: *Astrophys. J.* 130, p. 364. DOI: 10.1086/146726.

Babcock, H. W. (1961). „The Topology of the Sun's Magnetic Field and the 22-YEAR Cycle.“ In: *Astrophys. J.* 133, p. 572. DOI: 10.1086/147060.

Baliunas, S. L. et al. (1995). „Chromospheric variations in main-sequence stars“. In: *Astrophys. J.* 438, pp. 269–287. DOI: 10.1086/175072.

Berdyugina, S. V., J. Pelt, and I. Tuominen (2002). „Magnetic activity in the young solar analog LQ Hydrae. I. Active longitudes and cycles“. In: *A&A* 394, pp. 505–515. DOI: 10.1051/0004-6361:20021179.

Berdyugina, Svetlana V. (2005). „Starspots: A Key to the Stellar Dynamo“. In: *Living Reviews in Solar Physics* 2.1, p. 8. ISSN: 1614-4961. DOI: 10.12942/lrsp-2005-8. URL: http://dx.doi.org/10.12942/lrsp-2005-8.

Biermann, L. (1948). „Über die Ursache der chromosphärischen Turbulenz und des UV-Exzesses der Sonnenstrahlung“. In: *Z. Astrophys.* 25, p. 161.

Brandenburg, A., S. H. Saar, and C. R. Turpin (1998). „Time Evolution of the Magnetic Activity Cycle Period“. In: *Astrophys. J. Lett.* 498, pp. L51–L54. DOI: 10.1086/311297.

Budding, E. (1977). „Optimal curve fitting procedures applied to the light curves of classical Cepheids“. In: *Astrophysics and Space Science* 48, pp. 249–266. DOI: 10.1007/BF00648114.

Carrington, R. C. (1858). „On the Distribution of the Solar Spots in Latitudes since the Beginning of the Year 1854, with a Map“. In: *Monthly Notices of the Royal Academy of Science* 19, pp. 1–3. DOI: 10.1093/mnras/19.1.1.

Cayrel de Strobel, G. (1996). „Stars resembling the Sun“. In: 7, pp. 243–288. DOI: 10.1007/s001590050006.

Chadney, J. et al. (2014). „Modelling of Hot Jupiter thermospheres and ionospheres under irradiation from active stars“. In: *European Planetary Science Congress 2014, EPSC Abstracts, Vol. 9, id. EPSC2014-579* 9, EPSC2014-579, EPSC2014–579.

Chadney, J. M. et al. (2015). „XUV-driven mass loss from extrasolar giant planets orbiting active stars“. In: 250, pp. 357–367. DOI: 10.1016/j.icarus.2014.12.012. arXiv: 1412.3380 [astro-ph.SR].

Charbonneau, P. (2013). „Solar and Stellar Dynamos“. In: *Solar and Stellar Dynamos: Saas-Fee Advanced Course 39 Swiss Society for Astrophysics and Astronomy, Saas-Fee Advanced Courses, Volume 39. ISBN 978-3-642-32092-7. Springer-Verlag Berlin Heidelberg, 2013* 39. DOI: 10.1007/978-3-642-32093-4.

Cochran, W. D., A. P. Hatzes, and T. J. Hancock (1991). „Constraints on the companion object to HD 114762“. In: 380, pp. L35–L38. DOI: 10.1086/186167.

Deutsch, A. J. (1958). „Harmonic Analysis of the Periodic Spectrum Variables“. In: *Electromagnetic Phenomena in Cosmical Physics*. Ed. by B. Lehnert. Vol. 6. IAU Symposium, p. 209.

Donati, J.-F. and S. F. Brown (1997). „Zeeman-Doppler imaging of active stars. V. Sensitivity of maximum entropy magnetic maps to field orientation.“ In: *A&A* 326, pp. 1135–1142.

Dorren, J. D. (1987). „A new formulation of the starspot model, and the consequences of starspot structure“. In: *Astrophysical Journal* 320, pp. 756–767. DOI: 10.1086/165593.

Dorren, J. D. and E. F. Guinan (1994a). „HD 129333: The Sun in its infancy“. In: *Astrophysical J.* 428, pp. 805–818. DOI: 10.1086/174289.

— (1994b). „The Sun in Time: Detecting and Modelling Magnetic Inhomogenities on Solar-Type Stars“. In: *Poster Proceedings from IAU Colloquium 143: The Sun as a Variable Star: Solar and Stellar Irradiance Variations*. Ed. by J. M. Pap et al., p. 206.

Duncan, D. K. et al. (1991). „CA II H and K measurements made at Mount Wilson Observatory, 1966-1983“. In: *Astrophys. J. Suppl. Ser.* 76, pp. 383–430. DOI: 10.1086/191572.

Erkaev, N. V. et al. (2013). „XUV-Exposed, Non-Hydrostatic Hydrogen-Rich Upper Atmospheres of Terrestrial Planets. Part I: Atmospheric Expansion and Thermal Escape“. In: *Astrobiology* 13, pp. 1011–1029. DOI: 10.1089/ast.2012.0957. arXiv: 1212.4982 [astro-ph.EP].

Fontenla, J. M., E. H. Avrett, and R. Loeser (1990). „Energy balance in the solar transition region. I - Hydrostatic thermal models with ambipolar diffusion“. In: *Astrophys. J.* 355, pp. 700–718. DOI: 10.1086/168803.

— (1991). „Energy balance in the solar transition region. II - Effects of pressure and energy input on hydrostatic models“. In: *Astrophys. J.* 377, pp. 712–725. DOI: 10.1086/170399.

— (1993). „Energy balance in the solar transition region. III - Helium emission in hydrostatic, constant-abundance models with diffusion“. In: *Astrophys. J.* 406, pp. 319–345. DOI: 10.1086/172443.

— (2002). „Energy Balance in the Solar Transition Region. IV. Hydrogen and Helium Mass Flows with Diffusion“. In: *Astrophys. J.* 572, pp. 636–662. DOI: 10.1086/340227. eprint: astro-ph/0109416.

Fontenla, J. M., P. C. Stancil, and E. Landi (2015). „Solar Spectral Irradiance, Solar Activity, and the Near-Ultra-Violet“. In: *Astrophys. J.* 809, 157, p. 157. DOI: 10.1088/0004-637X/809/2/157.

Fontenla, J. M. et al. (2006). „Semiempirical Models of the Solar Atmosphere. I. The Quiet- and Active Sun Photosphere at Moderate Resolution“. In: *Astrophys. J.* 639, pp. 441–458. DOI: 10.1086/499345.

Fontenla, J. M. et al. (2009). „Semiempirical Models of the Solar Atmosphere. III. Set of Non-LTE Models for Far-Ultraviolet/Extreme-Ultraviolet Irradiance Computation“. In: *Astrophys. J.* 707, pp. 482–502. DOI: 10.1088/0004-637X/707/1/482.

Fontenla, J. M. et al. (2011). „High-resolution solar spectral irradiance from extreme ultraviolet to far infrared“. In: *Journal of Geophysical Research (Atmospheres)* 116, D20108, p. D20108. DOI: 10.1029/2011JD016032.

Fontenla, J. M. et al. (2014). „Far- and Extreme-UV Solar Spectral Irradiance and Radiance from Simplified Atmospheric Physical Models“. In: *Solar Physics* 289, pp. 515–544. DOI: 10.1007/s11207-013-0431-4.

Foukal, P. (1993). „The Curious Case of the Greenwich Faculae“. In: *Solar Physics* 148, pp. 219–232. DOI: 10.1007/BF00645087.

— (1998). „What Determines the Relative Areas of Spots and Faculae on Sun-like Stars?“ In: *Astrophys. J.* 500, pp. 958–965. DOI: 10.1086/305764.

Girardi, L. et al. (2002). „Theoretical isochrones in several photometric systems. I. Johnson-Cousins-Glass, HST/WFPC2, HST/NICMOS, Washington, and ESO Imaging Survey filter sets“. In: *A&A* 391, pp. 195–212. DOI: 10.1051/0004-6361:20020612. eprint: astro-ph/0205080.

Goncharskii, A. V. et al. (1977). „Reconstruction of local line profiles from those observed in an Ap spectrum.“ In: *Soviet Astronomy Letters* 3, pp. 147–149.

Gray, D. F. and S. L. Baliunas (1997). „The Rotation of the G0 Dwarf β Comae“. In: 475, pp. 303–312. DOI: 10.1086/303522.

Gray, R. O. et al. (2006). „Contributions to the Nearby Stars (NStars) Project: Spectroscopy of Stars Earlier than M0 within 40 pc-The Southern Sample“. In: *Astron. J.* 132, pp. 161–170. DOI: 10.1086/504637. eprint: astro-ph/0603770.

Güdel, M. (2004). „X-ray astronomy of stellar coronae“. In: 12, pp. 71–237. DOI: 10.1007/s00159-004-0023-2. eprint: astro-ph/0406661.

Güdel, M., E. F. Guinan, and S. L. Skinner (1997). „The X-Ray Sun in Time: A Study of the Long-Term Evolution of Coronae of Solar-Type Stars“. In: *Astrophys. J* 483, pp. 947–960. DOI: 10.1086/304264.

Guo, J. H. and L. Ben-Jaffel (2016). „The Influence of the Extreme Ultraviolet Spectral Energy Distribution on the Structure and Composition of the Upper Atmosphere of Exoplanets“. In: 818, 107, p. 107. DOI: 10.3847/0004-637X/818/2/107. arXiv: 1512.06470 [astro-ph.EP].

Hale, G. E. et al. (1919). „The Magnetic Polarity of Sun-Spots“. In: *Astrophys. J.* 49, p. 153. DOI: 10.1086/142452.

Hall, J. C. (2008). „Stellar Chromospheric Activity“. In: *Living Reviews in Solar Physics* 5, 2, p. 2. DOI: 10.12942/lrsp-2008-2.

Hall, J. C., G. W. Lockwood, and B. A. Skiff (2007). „The Activity and Variability of the Sun and Sun-like Stars. I. Synoptic Ca II H and K Observations“. In: *Astron. J.* 133, pp. 862–881. DOI: 10.1086/510356.

Hathaway, D. H. (2010). „The Solar Cycle“. In: *Living Reviews in Solar Physics* 7, 1, p. 1. DOI: 10.12942/lrsp-2010-1.

— (2013). „A Curious History of Sunspot Penumbrae“. In: *Solar Physics* 286, pp. 347–356. DOI: 10.1007/s11207-013-0291-y. arXiv: 1304.8060 [astro-ph.SR].

Henry, T. J. et al. (1996). „A Survey of Ca II H and K Chromospheric Emission in Southern Solar-Type Stars“. In: *Astron. J.* 111. DOI: 10.1086/117796.

Hoffleit, D., M. Saladyga, and P. Wlasuk (1983). *A Supplement to the Bright Star Catalogue. Containing data compiled through 1981 for stars 7.10 V and brighter that are not in the Bright Star Catalogue.*

Huebner, W. F. and C. W. Carpenter (1979). „Solar photo rate coefficients“. In: *NASA STI/Recon Technical Report N* 80.

Huebner, W. F. and J. Mukherjee (2015). „Photoionization and photodissociation rates in solar and blackbody radiation fields“. In: 106, pp. 11–45. DOI: 10.1016/j.pss.2014.11.022.

Johnstone, C. P. and M. Güdel (2015). „The coronal temperatures of low-mass main-sequence stars“. In: *A&A* 578, A129, A129. DOI: 10.1051/0004-6361/201425283. arXiv: 1505.00643 [astro-ph.SR].

Johnstone, C. P. et al. (2015). „The Evolution of Stellar Rotation and the Hydrogen Atmospheres of Habitable-zone Terrestrial Planets“. In: 815, L12, p. L12. DOI: 10.1088/2041-8205/815/1/L12. arXiv: 1511.03647 [astro-ph.EP].

King, J. R. et al. (2003). „Stellar Kinematic Groups. II. A Reexamination of the Membership, Activity, and Age of the Ursa Major Group“. In: 125, pp. 1980–2017. DOI: 10.1086/368241.

Kislyakova, K. G. et al. (2013). „XUV-Exposed, Non-Hydrostatic Hydrogen-Rich Upper Atmospheres of Terrestrial Planets. Part II: Hydrogen Coronae and Ion Escape“. In: *Astrobiology* 13, pp. 1030–1048. DOI: 10.1089/ast.2012.0958. arXiv: 1212.4710 [astro-ph.EP].

Kislyakova, K. G. et al. (2014). „Stellar wind interaction and pick-up ion escape of the Kepler-11 “super-Earths”“. In: 562, A116, A116. DOI: 10.1051/0004-6361/201322933. arXiv: 1312.4721 [astro-ph.EP].

Kjurkchieva, Diana P. (1990). „Photometry of stars with nonhomogeneous temperature spots“. In: *Astrophysics and Space Science* 172.2, pp. 255–262. ISSN: 1572-946X. DOI: 10.1007/BF00643317. URL: http://dx.doi.org/10.1007/BF00643317.

Koskinen, T. T. et al. (2013). „The escape of heavy atoms from the ionosphere of HD209458b. I. A photochemical-dynamical model of the thermosphere“. In: 226, pp. 1678–1694. DOI: 10.1016/j.icarus.2012.09.027. arXiv: 1210.1536 [astro-ph.EP].

Lammer, H. et al. (2014). „Origin and loss of nebula-captured hydrogen envelopes from ‘sub’- to ‘super-Earths’ in the habitable zone of Sun-like stars“. In: 439, pp. 3225–3238. DOI: 10.1093/mnras/stu085. arXiv: 1401.2765 [astro-ph.EP].

Latham, D. W. et al. (1989). „The unseen companion of HD114762 - A probable brown dwarf“. In: 339, pp. 38–40. DOI: 10.1038/339038a0.

Lean, J. L. et al. (2001). „Variability of a composite chromospheric irradiance index during the 11-year activity cycle and over longer time periods“. In: *Journal of Geophysics Research* 106, pp. 10645–10658. DOI: 10.1029/2000JA000340.

Lichtenegger, H. I. M. et al. (2010). „Aeronomical evidence for higher CO_2 levels during Earths Hadean epoch“. In: 210, pp. 1–7. DOI: 10.1016/j.icarus.2010.06.042.

Luger, R. et al. (2015). „Habitable Evaporated Cores: Transforming Mini-Neptunes into Super-Earths in the Habitable Zones of M Dwarfs“. In: *Astrobiology* 15, pp. 57–88. DOI: 10.1089/ast.2014.1215. arXiv: 1501.06572 [astro-ph.EP].

Maggio, A. et al. (1987). „Einstein Observatory survey of X-ray emission from solar-type stars - The late F and G dwarf stars“. In: *Astrophys. J.* 315, pp. 687–699. DOI: 10.1086/165170.

Mathieu, R. D. and T. Mazeh (1988). „The circularized binaries in open clusters - A new clock for age determination“. In: 326, pp. 256–264. DOI: 10.1086/166087.

Mayor, M. and D. Queloz (1995). „A Jupiter-mass companion to a solar-type star“. In: 378, pp. 355–359. DOI: 10.1038/378355a0.

Messina, S. and E. F. Guinan (2002). „Magnetic activity of six young solar analogues I. Starspot cycles from long-term photometry“. In: *A&A* 393, pp. 225–237. DOI: 10.1051/0004-6361:20021000.

— (2003). „Magnetic activity of six young solar analogues II. Surface Differential Rotation from long-term photometry“. In: *A&A* 409, pp. 1017–1030. DOI: 10.1051/0004-6361:20031161.

Messina, S., E.F. Guinan, and A.F. Lanza (1998). „Photospheric Magnetic Activity in a Proxy for the Young Sun: HD 134319“. In: *Astrophysics and Space Science* 260.4, pp. 493–505. ISSN: 1572-946X. DOI: 10.1023/A:1001745231017. URL: http://dx.doi.org/10.1023/A:1001745231017.

Messina, S., M. Rodonò, and E. F. Guinan (2001). „The “rotation-activity connection”: Its extension to photospheric activity diagnostics“. In: *A&A* 366, pp. 215–228. DOI: 10.1051/0004-6361:20000201.

Middelkoop, F. (1982). „Magnetic structure in cool stars. IV - Rotation and CA II H and K emission of main-sequence stars“. In: *Astronomy & Astrophysics.* 107, pp. 31–35.

Montes, D. et al. (2001a). „Chromospheric activity, lithium and radial velocities of single late-type stars possible members of young moving groups“. In: *A&A* 379, pp. 976–991. DOI: 10.1051/0004-6361:20011385. eprint: astro-ph/0110066.

Montes, D. et al. (2001b). „Late-type members of young stellar kinematic groups - I. Single stars“. In: *MNRAS* 328, pp. 45–63. DOI: 10.1046/j.1365-8711.2001.04781.x. eprint: astro-ph/0106537.

Neff, J. E., D. O'Neal, and S. H. Saar (1995). „Absolute Measurements of Starspot Area and Temperature: II Pegasi in 1989 October“. In: *Astrophysical Journal* 452, p. 879. DOI: 10.1086/176356.

Noyes, R. W. et al. (1984). „Rotation, convection, and magnetic activity in lower main-sequence stars“. In: *Astrophys. J.* 279, pp. 763–777. DOI: 10.1086/161945.

O'Neal, D. et al. (2004). „Further Results of TiO-Band Observations of Starspots“. In: *Astronomical J.* 128, pp. 1802–1811. DOI: 10.1086/423438.

Parker, D. E., C. K. Folland, and M. Jackson (1995). „Marine surface temperature: Observed variations and data requirements“. In: *Climatic Change* 31.2, pp. 559–600. ISSN: 1573-1480. DOI: 10.1007/BF01095162. URL: http://dx.doi.org/10.1007/BF01095162.

Peres, G. et al. (2000). „The Sun as an X-Ray Star. II. Using theYohkoh/Soft X-Ray Telescope-derived Solar Emission Measure versus Temperature to Interpret Stellar X-Ray Observations“. In: *Astrophys. J* 528, pp. 537–551. DOI: 10.1086/308136.

Radick, R. R. et al. (1998). „Patterns of Variation among Sun-like Stars“. In: *Astrophys. J. Suppl. Ser.* 118, pp. 239–258. DOI: 10.1086/313135.

Ribas, I. et al. (2005). „Evolution of the Solar Activity over Time and Effects on Planetary Atmospheres. I. High-Energy Irradiances (1-1700 Å)“. In: *Astrophys. J.* 622, pp. 680–694. DOI: 10.1086/427977. eprint: astro-ph/0412253.

Rodono, M. et al. (1986). „Rotational modulation and flares on RS CVn and BY Dra-type stars. I - Photometry and SPOT models for BY Dra, AU Mic, AR Lac, II Peg and V 711 Tau (= HR 1099)“. In: *A&A* 165, pp. 135–156.

Rosén, L., O. Kochukhov, and G. A. Wade (2015). „First Zeeman Doppler Imaging of a Cool Star Using all Four Stokes Parameters“. In: 805, 169, p. 169. DOI: 10.1088/0004-637X/805/2/169. arXiv: 1504.00176 [astro-ph.SR].

Saar, S. H. and A. Brandenburg (1999). „Time Evolution of the Magnetic Activity Cycle Period. II. Results for an Expanded Stellar Sample“. In: *Astrophys. J.* 524, pp. 295–310. DOI: 10.1086/307794.

Sanz-Forcada, J. et al. (2011). „Planet erosion by coronal radiation“. In: *Highlights of Spanish Astrophysics VI*. Ed. by M. R. Zapatero Osorio et al., pp. 607–612.

Schwabe, M. (1844). „Sonnenbeobachtungen im Jahre 1843. Von Herrn Hofrath Schwabe in Dessau“. In: *Astronomische Nachrichten* 21, p. 233.

Schwarzschild, M. (1948). „On Noise Arising from the Solar Granulation.“ In: *Astrophys. J.* 107, p. 1. DOI: 10.1086/144983.

Semel, M. (1989). „Zeeman-Doppler imaging of active stars. I - Basic principles“. In: *A&A* 225, pp. 456–466.

Semel, M. and J. Li (1996). „Zeeman-Doppler Imaging of Solar-Type Stars: Multi Line Technique“. In: *Solar Physics* 164, pp. 417–428. DOI: 10.1007/BF00146653.

Shaikhislamov, I. F. et al. (2014). „Atmosphere Expansion and Mass Loss of Close-orbit Giant Exoplanets Heated by Stellar XUV. I. Modeling of Hydrodynamic Escape of Upper Atmospheric Material“. In: 795, 132, p. 132. DOI: 10.1088/0004-637X/795/2/132. arXiv: 1506.03548 [astro-ph.EP].

Shapiro, A. I. et al. (2014). „Variability of Sun-like stars: reproducing observed photometric trends“. In: *A&A* 569, A38, A38. DOI: 10.1051/0004-6361/201323086. arXiv: 1406.2383 [astro-ph.SR].

Shematovich, V. I., D. E. Ionov, and H. Lammer (2014). „Heating efficiency in hydrogen-dominated upper atmospheres“. In: 571, A94, A94. DOI: 10.1051/0004-6361/201423573. arXiv: 1409.0730 [astro-ph.EP].

Skumanich, A. (1972). „Time Scales for CA II Emission Decay, Rotational Braking, and Lithium Depletion“. In: *Astrophys. J.* 171, p. 565. DOI: 10.1086/151310.

Smith, R. K. et al. (2001). „Collisional Plasma Models with APEC/APED: Emission-Line Diagnostics of Hydrogen-like and Helium-like Ions“. In: *Astrophys. J. Lett.* 556, pp. L91–L95. DOI: 10.1086/322992. eprint: astro-ph/0106478.

Soderblom, D. R. and M. Mayor (1993). „Stellar kinematic groups. I - The Ursa Major group“. In: 105, pp. 226–249. DOI: 10.1086/116422.

Soderblom, D. R. et al. (1993). „The evolution of angular momentum among zero-age main-sequence solar-type stars“. In: *Astrophys. J.* 409, pp. 624–634. DOI: 10.1086/172694.

Solanki, S. K. and M. Fligge (1998). „Solar irradiance since 1874 revisited“. In: *Geophysics Research Letters* 25, pp. 341–344. DOI: 10.1029/98GL50038.

Solanki, S. K. and N. A. Krivova (2003). „Can solar variability explain global warming since 1970?“ In: *Journal of Geophysical Research (Space Physics)* 108, 1200, p. 1200. DOI: 10.1029/2002JA009753.

Strassmeier, K. G. (1988). „A multiple SPOT model for simultaneous solution of light curves and distorted line profiles of spotted stars“. In: *Astrophysics and Space Science* 140, pp. 223–235. DOI: 10.1007/BF00638982.

— (2009). „Starspots“. In: *A&A Reviews* 17, pp. 251–308. DOI: 10.1007/s00159-009-0020-6.

Strassmeier, K. G. and B. W. Bopp (1992). „Time-series photometric SPOT modeling. I - Parameter study and application to HD 17433 = VY ARIETIS“. In: *A&A* 259, pp. 183–197.

Strassmeier, K. G. and J. B. Rice (1998). „Doppler imaging of stellar surface structure. VI. HD 129333 = EK Draconis: a stellar analog of the active young Sun“. In: *A&A* 330, pp. 685–695.

Telleschi, A. et al. (2005). „Coronal Evolution of the Sun in Time: High-Resolution X-Ray Spectroscopy of Solar Analogs with Different Ages“. In: *Astrophys. J.* 622, pp. 653–679. DOI: 10.1086/428109. eprint: astro-ph/0503546.

Thejll, P. and K. Lassen (2000). „Solar forcing of the Northern hemisphere land air temperature: New data“. In: *Journal of Atmospheric and Solar-Terrestrial Physics* 62, pp. 1207–1213. DOI: 10.1016/S1364-6826(00)00104-8.

Tian, F. et al. (2005). „Transonic Hydrodynamic Escape of Hydrogen from Extrasolar Planetary Atmospheres“. In: 621, pp. 1049–1060. DOI: 10.1086/427204.

Tian, F. et al. (2008). „Hydrodynamic planetary thermosphere model: 1. Response of the Earth's thermosphere to extreme solar EUV conditions and the significance of adiabatic cooling“. In: *Journal of Geophysical Research (Planets)* 113, E05008, E05008. DOI: 10.1029/2007JE002946.

Tu, L. et al. (2015). „The extreme ultraviolet and X-ray Sun in Time: High-energy evolutionary tracks of a solar-like star“. In: 577, L3, p. L3. DOI: 10.1051/0004-6361/201526146. arXiv: 1504.04546 [astro-ph.SR].

Vaughan, A. H. and G. W. Preston (1980). „A survey of chromospheric CA II H and K emission in field stars of the solar neighborhood“. In: *Publ. Astron. Soc. Pac* 92, pp. 385–391. DOI: 10.1086/130683.

Vaughan, A. H., G. W. Preston, and O. C. Wilson (1978). „Flux measurements of CA II H and K emission“. In: *Publ. Astron. Soc. Pac* 90, pp. 267–274. DOI: 10.1086/130324.

Vaughan, A. H. et al. (1981). „Stellar rotation in lower main-sequence stars measured from time variations in H and K emission-line fluxes. I - Initial results“. In: *Astrophys. J.* 250, pp. 276–283. DOI: 10.1086/159372.

Vernazza, J. E., E. H. Avrett, and R. Loeser (1981). „Structure of the solar chromosphere. III - Models of the EUV brightness components of the quiet-sun“. In: *Astrophys. J. Suppl. Ser.* 45, pp. 635–725. DOI: 10.1086/190731.

Vogt, S. S. (1981). „A method for unambiguous determination of starspot temperatures and areas - Application to II Pegasi, BY Draconis, and HD 209813“. In: *Astrophysical Journal* 250, pp. 327–340. DOI: 10.1086/159379.

Vogt, S. S. and G. D. Penrod (1983). „Detection of high-order nonradial oscillations on the rapid rotator Zeta Ophiuchi and their link with Be type outbursts“. In: *Astrophysical Journal* 275, pp. 661–682. DOI: 10.1086/161564.

Wichmann, R., J. H. M. M. Schmitt, and S. Hubrig (2003). „Nearby young stars“. In: *A&A* 399, pp. 983–994. DOI: 10.1051/0004-6361:20021867.

Wilson, O. C. (1978). „Chromospheric variations in main-sequence stars“. In: *Astrophys. J.* 226, pp. 379–396. DOI: 10.1086/156618.

Wolf, R. (1861). „Abstract of his latest Results“. In: *MNRAS* 21, p. 77. DOI: 10.1093/mnras/21.3.77.

Wright, N. J. et al. (2011). „The Stellar-activity-Rotation Relationship and the Evolution of Stellar Dynamos“. In: 743, 48, p. 48. DOI: 10.1088/0004-637X/743/1/48. arXiv: 1109.4634 [astro-ph.SR].